

## Article

# Exploitation of a New Short-Term Multimodel Photovoltaic Power Forecasting Method in the Very Short-Term Horizon to Derive a Multi-Time Scale Forecasting System

Elena Collino \* and Dario Ronzio

RSE S.p.A.—Ricerca sul Sistema Energetico, Via Rubattino 54, 20134 Milano, Italy; dario.ronzio@rse-web.it  
\* Correspondence: elena.collino@rse-web.it; Tel.: +39-02-39925653

**Abstract:** The relentless spread of photovoltaic production drives searches of smart approaches to mitigate unbalances in power demand and supply, instability on the grid and ensuring stable revenues to the producer. Because of the development of energy markets with multiple time sessions, there is a growing need of power forecasting for multiple time steps, from fifteen minutes up to days ahead. To address this issue, in this study both a short-term-horizon of three days and a very-short-term-horizon of three hours photovoltaic production forecasting methods are presented. The short-term is based on a multimodel approach and referred to several configurations of the Analog Ensemble method, using the weather forecast of four numerical weather prediction models. The very-short-term consists of an Auto-Regressive Integrated Moving Average Model with exogenous input (ARIMAX) that uses the short-term power forecast and the irradiance from satellite elaborations as exogenous variables. The methods, applied for one year to four small-scale grid-connected plants in Italy, have obtained promising improvements with respect to reference methods. The time horizon after which the short-term was able to outperform the very-short-term has also been analyzed. The study also revealed the usefulness of satellite data on cloudiness to properly interpret the results of the performance analysis.

**Keywords:** photovoltaic power forecast; Analog Ensemble; ARIMAX; multimodel; satellite data; numerical weather prediction; forecasting skill; short-term; very-short-term



**Citation:** Collino, E.; Ronzio, D. Exploitation of a New Short-Term Multimodel Photovoltaic Power Forecasting Method in the Very Short-Term Horizon to Derive a Multi-Time Scale Forecasting System. *Energies* **2021**, *14*, 789. <https://doi.org/10.3390/en14030789>

Academic Editors: Emanuele Ogliari and Sonia Leva

Received: 20 December 2020

Accepted: 25 January 2021

Published: 2 February 2021

**Publisher's Note:** MDPI stays neutral with regard to jurisdictional claims in published maps and institutional affiliations.



**Copyright:** © 2021 by the authors. Licensee MDPI, Basel, Switzerland. This article is an open access article distributed under the terms and conditions of the Creative Commons Attribution (CC BY) license (<https://creativecommons.org/licenses/by/4.0/>).

## 1. Introduction

Energy sector has undergone rapid and substantial transformations during the last decade, both in terms of energy production and consumption. The increase in global energy demand on the one hand and the necessity to mitigate the dramatic effects of climate change, on the other hand, have forced researchers, policymakers and economists to look for new energy production systems, less dependent on exhaustible sources, more efficient and characterized by low emissions of greenhouse components into the atmosphere. Ambitious commitments have been taken during the United Nations Climate Change Conference (COP21) in 2015, to limit global warming to well below 2° Celsius. In order to reach this result, a decarbonization in the energy production system is underway. Green energy incentives and the progressive and continuous decrease of solar and wind costs [1], have led to a huge deployment of renewable plants worldwide. 2019 marked a record with 200 GW of renewable power added globally [1], 115 of which were solar installations. The beginning of 2020, despite the global reduction in energy demand, due to COVID-19, saw an increase in renewable power demand [2]. In the same period, a record in the share of solar and wind production in the electricity demand was experienced in many countries, undermining the safety and the stability of the transmission and distribution grid, due to the inherent variability of these sources. It is well known, in fact, that the production of solar and wind plants is mainly affected by weather conditions, causing sudden variations in production profiles and requiring rapid actions by grid operators in

order to mitigate imbalances between demand and supply of energy. This results in an increase of flexible energy reserve to address imbalances and additional uncertainty in the energy market. By means of an accurate forecasting of power production, the benefits of using renewable sources over fossil-fired power plants will increase to an ever-greater extent. In addition to undoubted advantages for the environment, in terms of avoided CO<sub>2</sub> emissions, solar renewable production is profitable for the producer first of all because the fuel is free and inexhaustible. Furthermore, in many countries there are lots of incentives to promote renewable energy projects. For example, in Europe the Cohesion Fund allocated a total of €63.4 billion to promote sustainable development between 2014 and 2020 in some European countries and around €5.9 billion have been devoted towards energy research and innovation projects in the European Union Horizon 2020 program. At present, the convenience in using fossil-fired sources appears to result from the possibility to tune the production according to the short-time power demand. Actually, with an accurate production forecast, updated several times a day, it is possible to optimize the management of ancillary systems to supply energy in case of demand peaks, allowing to choose the most convenient production system according to the current scenario of power demand and supply. Accurate forecasting also allows for better management of storage systems that can be coupled with solar plants, making it more profitable. Finally, in many countries, penalties are applied when inaccurate power predictions plans are submitted, and the economic value of accurate forecasting has been investigated by Antonanzas et al. [3] and Reindl et al. [4].

The variability of nonprogrammable renewable sources affects different time scales, with several impacts. For example, the precise knowledge on the future renewable energy (RE) profile in the range of minutes is particularly beneficial for real time dispatch operation, storage control, grid stability management [5]. The variability in the next few hours is closely related to energy trading in the intraday market, along with the management of storage devices and dispatching operations [6]. The RE profile for the subsequent days mainly applies to planning purposes and to formulate bids for electricity markets [4,7].

According to the forecast horizon, various approaches have been developed up to now, using different types of input data. Recent comprehensive reviews of PhotoVoltaic (PV) solar power forecasting techniques can be obtained from Das et al. [5], Mellit et al. [8], Ahmed et al. [9]. In particular, in the review by Ahmed et al. [9] there is a discussion on the terms used to define the forecast horizon and there is an attempt to classify the forecasting techniques in categories: persistence forecasting, physical models, statistical techniques. It is important to note that the expression “physical approach” is often used with different meaning. In the same review [9], for example, it relates to the use of Numerical Weather Prediction models (*NWP*) to forecast the meteorological variables affecting renewable production. It is necessary to be aware that *NWP* do not provide production forecasts, but they solve the integrodifferential equations describing the state of the atmosphere and soil/land/sea/ atmosphere interactions at different spatial scales. As output, they also predict the values of the meteorological variables affecting RE production. It is always necessary a postprocessing to convert weather information in production forecast. In this case, the final power forecast will be derived with two possible ways: by means of a statistical technique that uses in input *NWP* forecasts, such as Artificial Neural Network (ANN), Support Vector Machine (SVM) and so forth, or by using the same information to feed a specific model of the plant, describing system size, module and array type, system losses, inverter efficiency and so on. Some authors refer to the latter type of model, that is a detailed simulation of the real plant, as the physical approach [10]. Therefore, it is necessary to pay close attention to the meaning of the words used in this field by authors with different backgrounds. There are many and varied techniques exploited so far to derive PV power forecasting. The simplest one is the persistence forecast, which is considered an accurate and cost-effective forecasting system in the range of 0–15 min ahead by many authors, such as Dutta et al. [11], Barbieri et al. [12] and Zhou et al. [13]. Another group of forecasting systems includes time series based forecasting techniques, such as

exponential smoothing methods, autoregressive moving average (ARMA), autoregressive integrated moving average (ARIMA), as reported by Pedro et al. [14], Ahmad et al. [15], Nobre et al. [16]. These methods predict the forthcoming value of a variable by evaluating the pattern of the same variable in the past. They are characterized by the absence of exogenous inputs. ARIMA models, with respect to ARMA models, have the capability of clipping nonstationary values from the data. These methods have been implemented for both sub-hourly and day-ahead forecasting horizons. ARIMA is often used as reference method. Time series methods have the undoubted advantage of being very fast. However, the main drawback is the lack of physical modelling during the forecasting process, such as the absence of weather information. This issue can be addressed with the multivariate versions of time series models, such as the Auto-Regressive Integrated Moving Average Model with exogenous input (ARIMAX). To the best of authors' knowledge, only few authors have explored the latter methodology for PV power forecasting applications, such as Zhou et al. [13], Bacher et al. [17], Perez-Mora et al. [18] and Li et al. [19], even if it seems a cost-effective forecasting system with good performances.

The most popular methods used in PV power forecasting exploit machine learning (ML) techniques. This approach refers to the ability of computers to learn from experience, without being programmed by human beings, as described by Samuel A.L. [20]. They include Artificial Neural Networks (ANN) with their ability to approximate nonlinear functions. The ANN architecture consists of a network of connected artificial neurons in different layers: the input, the hidden (multiple levels are possible), and the output layer. The neuron consists of input(s), net function, transfer function, and output(s). There are lots of different types of ANN with different architectures used to derive PV power forecasting [14,21,22]. A subset of ML techniques is the Deep Learning (DL), referring to the ability of deep neural networks of learning from voluminous input data and numerous hidden layers, as specified by Deng and Yu [23]. Convolutional Neural Network (CNN) [24], Long Short Term Memory (LSTM) [13,25,26], multilayer perceptron (MLP) [27], recurrent neural network (RNN) [28,29] are the principal DL methods. A specific recent review of ML and DL methods applied to PV power forecasting is presented by Mellit et al. [8]. These methods are considered promising and accurate when implemented with a large training dataset. They often require pretreatments of the dataset, to exclude outliers and wrong data. They may experience overfitting problems and they are computation intensive. They need to be retrained when new data are available, therefore, for online application, for example with constant updates of the forecast during the day, they may not be the most efficient solution.

Another approach consists in the probabilistic forecast. With the probabilistic approach the output consists of a distribution of probability of the future values of power. The research in the probabilistic forecast of solar power production is generally considered immature at present. A review regarding this approach has been made by Van der Meer et al. [30]. The most popular probabilistic forecasting models are quantile regression-based methods, presented by Lauret et al. [31], and simulating predictors used by Kim et al. [32]. The probabilistic forecasting is often obtained by feeding simulated explanatory weather scenarios into a deterministic forecasting model. In this regard a recent work by Sun et al. [33] pointed out the importance of considering the correlation among different explanatory weather variables. This analysis can be performed when historical measured and forecasted weather data are available. In many countries the availability of weather measurements is rather limited, in part because they are managed by different companies and they are not available free of charge. Radiation measurements, in particular, are obtained from costly instruments and they are therefore even rarer. An alternative probabilistic approach that does not require weather measurements consists in the Analog Ensemble, implemented by Alessandrini et al. [34]. The Analog Ensemble (*AnEn*) is a statistical technique that uses the weather forecast predictors to identify the past events more similar to the current forecast. Once selected the time in which similar

weather forecast have occurred, a distribution of the forecasting variable is created using the past measurements of that variable recorded in those past times.

Up to now researchers have been mainly focused to derive the most accurate power forecasting tool for a specific forecast horizon, such as the very-short-term (15–180 min ahead) or the short-term (up to 72 h ahead), according to the final application of the forecasting.

At the moment, the interest in accurate production forecasts for multiple time frames, from few minutes in advance, till some days ahead, is growing more and more, especially for solar, due to its ever-increasing penetration in electricity grids. More and more often, photovoltaic plants are coupled with storage systems, in order to store surplus energy and eventually use the hybrid system for balancing purposes. Innovative technological solutions are being developed in this field, such as new photovoltaic panels with integrated lithium accumulators as suggested by Poulek et al. [35]. In this case, for the optimal management of the system, a real time PV power forecasting is necessary, especially to deal with ramps, but it is also important to know the production profile of the following days, in order to operate a smart management of the storage and because producers are often asked to supply the day-ahead production plan to prevent serious stability issues on the grid. Furthermore, the same producer may be interested in participating in both the intra-day and day-ahead energy market. This requirement is catching on in many countries, also because of the creation of aggregators of distributed solar producers, participating directly in electricity markets.

As regards the primary source, an analysis on the performance of different irradiance forecasting methods to varying of the spatial-time scale is reported by Diagne et al. [36]. On the basis of the fact that the main factor affecting PV production is the solar irradiation, as reported by Diagne et al. [36], Cai et al. [37], Liu et al. [38], it is usual to transfer the considerations derived from irradiance forecasting studies also in the PV forecasting field, but a corresponding analysis of the variation of the PV power forecasting performances when the forecasting horizon changes from few minutes until days ahead has not been performed yet.

On the other hand, the research in multiple time frames prediction is immature and according to Mellit et al. [8] the multistep prediction is a current challenge in the PV field. Mishra et al. [39] proposed an RNN-based approach to forecast the PV production from one hour till 4 h ahead. The method was implemented using lots of observed weather variables. It achieved low root mean square errors across all the forecasting time-horizons and brought out the relevance of multi-time horizon forecasting for industrial applications. This method has the drawback of the necessity of observed weather data, often not available close to the plant and covers a limited range of forecast. A more extended multistep prediction has been addressed by Carriere et al. [40], with a PV power forecasting spanning from five minutes till thirty-six hours ahead.

They have highlighted the reasons behind a PV power forecasting covering multiple time frames and proposed an approach based on the *AnEn* technique. In their work the same model was used along the time, fed with observed data, *NWP* forecasts and satellite information. The system was tested on large PV plants with performances comparable with the state-of-the-art approaches developed for specific time horizons. The strength of this approach is to use a single method for all the forecast horizons, even if this condition could lead to less accuracy for specific timeframe, with respect to use different methods, for different horizons.

In this work the implementation of a multistep PV power forecasting tool, covering the horizons from 15 min to three days ahead with a time resolution of fifteen minutes, has been addressed in a different way, by exploiting two different methods, one devoted to deriving an accurate forecast for the short-term (*ST*) horizon, till three days ahead and another one for the very-short-term horizon (*VST*), covering the period from 15 min till three hours in advance.

The ST forecasting is an original method, based on a multimodel approach, made of different configurations of an Analog Ensemble, fed with the weather forecast derived from various NWP models. The very-short-term PV power forecast is generated based on ARIMAX method, using the PV forecast derived from the ST prediction as explanatory variable.

With regard to the methods, *AnEn* has already revealed its strength in previous applications on PV power forecasting, compared to other state of art methods, such as quantile regression, as confirmed by Alessandrini et al. [34] and with respect to hybrid methods combining k-Nearest Neighbors and Quantile Regression Forest and a Multi-Layer Perceptron neural network, as studied in the benchmark on regional PV power forecasting models by Pierro et al. [41]. In addition to its performance, another advantage of this method is that it requires minimal computational resources. The novelty of the *AnEn* used in this work consists in the multimodel approach, derived from different configurations of the *AnEn*, as well as the use of more than just one NWP prediction model in input to the *AnEn*.

For the VST, the ARIMAX has been chosen because it is a fast algorithm, therefore it is appropriate for online use. It is able to rapidly adapt to changes in operational production, such as fell in production due to breaks of arrays or degradations of inverters. It does not need to be re-trained when new measurements are available. As regards its reliability, even though it has been under-exploited so far, it has proven to be able to provide better prediction performance than an NN model by Li et al. [19]. The ARIMAX implemented in this work has the peculiarity of using the output of the ST forecast as explanatory variable, in addition to two more exogenous variables, i.e., irradiation from satellite data and a smart power persistence of the PV power.

The main originality of the work lies in the exploitation of the results of the ST in the VST, as well as the use of a multimodel approach to improve the performance of the ST. The performance variations of the multimodel ST and VST along the entire forecasting time have been evaluated, in order to detect the time horizon after which the ST could outperform the VST.

It is well known that PV power production varies accordingly to irradiance variations, that may occur at different time scales—from seconds until decades—and the frequency of variations relies with the climate of the region where the PV plant is installed. For this reason, the same power forecasting method can achieve different accuracy levels, depending on the climatic conditions of the region where the plant is placed. In order to look into this matter, the developed PV power forecasting methods have been applied to four PV plants, located in various Italian regions, characterized by heterogeneous climate and orography. Italy, in fact, is a small country, but with a large variability in orography. Approximately 35% of the territory is mountainous, 40% hilly and is almost completely surrounded by the sea. This results in a large variety of microclimates and frequent variations in weather conditions. For this reason, the results have been specifically analyzed in view of the distribution of the cloudiness in correspondence of each site.

The work also aims at looking into several aspects of the forecasting performance, by means of the analysis of a wide range of error indexes, in order to provide an overall view on the prediction system in various climatic conditions.

Main contributions of this paper are summarized as follows:

- A new multi-time frames solar power forecasting method is developed by combining a ST and a VST forecasting system.
- The ST is based on a multimodel approach applied to the *AnEn* technique.
- The output of the ST is used as explanatory variable of ARIMAX in the VST.
- A smart power persistence forecast is introduced.
- The performances are evaluated in view of the cloudiness variability of the sites, exploiting meteorological satellite data.

The paper is organized as follows: in Section 2 a description of the plants on which the methods have been tested together with the data used in this work is given (Sections 2.1 and 2.2

respectively). In the same section, the implemented methods and the performance metrics are discussed (Sections 2.3 and 2.4 respectively). In Section 3 the results are analyzed, while Section 4 is devoted to a discussion on the results. The specific performance analysis in view of the cloudiness variation of the sites is reported in Appendix A.

## 2. Materials and Methods

### 2.1. Power Output

The PV power forecast for multiple time frames has been tested on four Italian small-scale grid-connected PV plants. The first plant, named P1, is located in the South of Italy, on flat terrain. Two other plants, named P2 and P3, are installed in central Italy. P2 is characterized by an installation in complex terrain, at an altitude of 900 m, whereas the last plant—P4—is placed in the North of Italy, in Liguria, a few kilometres from the sea. It is situated in a valley surrounded by relative high mountain ranges. Because of its position, it is characterized by peculiar climatic conditions. The siting of the plants, with the orography, is presented in Figure 1.



**Figure 1.** Location of the four PV plants used in the study.

The plants differ each other for size, typology of panels and orientation. In particular, P4 is oriented to East.

The main characteristics of the installations are summarized in Table 1.

**Table 1.** Main characteristics of the PV plants. Note that P4 has an exposition of 17° East.

Plant	Nominal Power (kWp)	Type	Orientation	Inclination
P1	14.76	mono c-Si	180°	30°
P2	49.68	mono c-Si	180°	30°
P3	19.8	Polycrystalline	180°	30°
P4	14.88	mono c-Si	163°	30°

15-min interval power data from 2016 to the end of 2019 from the four plants have been collected in order to develop and test the ST and the VST. In particular, the ST has been trained during the period July 2016–October 2018, while the multi-time frame system has been performed and tested during the period from November 2018 until November 2019. The test, performed over a complete year, enabled it to evaluate the performance of the method in different seasonal conditions. The dataset used for the test contains only day-time data, with a size of around 15,000 samples, depending on the availability of the power measurements during the year.

In Figure 2 the temporal evolution of the PV production and the corresponding Global Horizontal Irradiation (GHI), for the four plants, from July 2016 to November 2019 is shown.

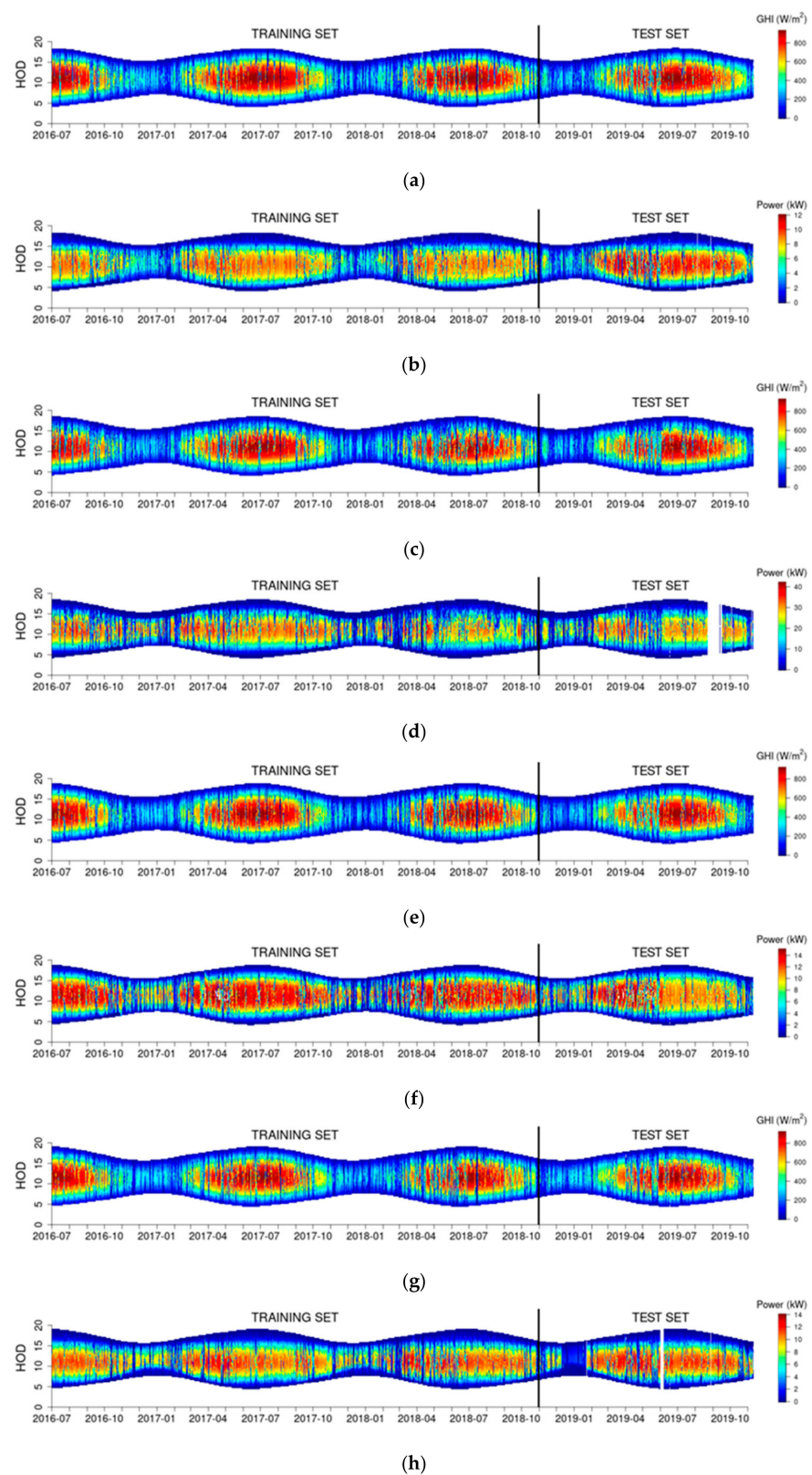


**Figure 2.** From top to bottom, heatmaps of Hour Of the Day vs. day of the year of measurements of (a) GHI of plant P1, (b) PV power production at the plant P1; (c) GHI of plant P2, (d) PV power production at the plant P2; (e) GHI of plant P3, (f) PV power production at the plant P3; (g) GHI of plant P4, (h) PV power production at the plant P4.

By comparing the temporal evolution of the production (graphs b, d, f, and h in Figure 2) with the progress of the GHI (graphs a, c, e, and g in the same figure), it is possible to note the strong relationship among these fields for all the plants except for plant P1 which underwent a revamp in 2019, so that its production in 2019 was higher than in previous years. On the contrary, plant P3 suffered inverter failure in May 2019, resulting in a reduction in production capacity.

It is also possible to notice the considerable variability in both inter- and intra-annual radiation and production. This simple comparison supplies a clear picture of the operational conditions that can occur and points out that a real-time forecasting method must try to quickly adapt to the always possible changes in the system characteristics as well as irradiance variations.

## 2.2. Meteorological Data

Different sources of meteorological information have been used in this study. Weather data have been used in part as predictors of the power forecasting methods and in part to evaluate the performance variations in function of the climatic properties of each site, as described in Section 3 and in Appendix A.

### 2.2.1. NWP Forecast

The forecast of the weather variables affecting PV production, used as input of the short-term PV forecast, has been derived from two different numerical weather prediction models: the Weather Research and Forecasting Model (*WRF*) [42] and the Regional Atmospheric Modeling System (*RAMS*) [43].

They are local area models, driven with initial and boundary conditions supplied by a global area model. The run of each local area model has been performed using two different global *NWP* models that provided the initial and boundary conditions. The used global *NWP* models are the Integrated Forecast System (*IFS*), developed by the European Centre for Medium Range Weather Forecasts, UK (ECMWF), and the Global Forecast System (*GFS*), developed by the National Oceanic and Atmospheric Administration, USA (NOAA).

In this study, both *WRF* and *RAMS* have been run once a day, with start at 12 UTC. Each run has supplied the weather forecast for the following three days, with a spatial resolution of 4 km and a time resolution of 1 h over a domain covering the Italian territory. For each PV plant, the weather forecast on the nearest *NWP* model point has been used and a temporal interpolation has been performed in order to obtain a fifteen-minute weather forecast up to three days ahead.

Because of the use of the two local area models and the two drivers, each weather variable has been forecasted by four different model chains, hereinafter referred to:

- $WGN = WRF + GFS$
- $WES = WRF + IFS$
- $RGN = RAMS + GFS$
- $RES = RAMS + IFS$

A scheme, to describe the four *NWP* chains, is reported in Figure 3.

The weather variables used to perform the short-term forecast are:

- Global Horizontal Irradiation (*GHI*)
- Diffuse Horizontal Irradiation (*DHI*)
- Direct Normal Irradiation (*DNI*)
- Wind speed at 10 m (*WS*)
- Relative Humidity (*RHU*)
- Panel Temperature (*TPAN*)
- Precipitable Water Content (*PWC*)

Some considerations about the choice of the weather input for the *ST* are reported in Section 2.3.1.

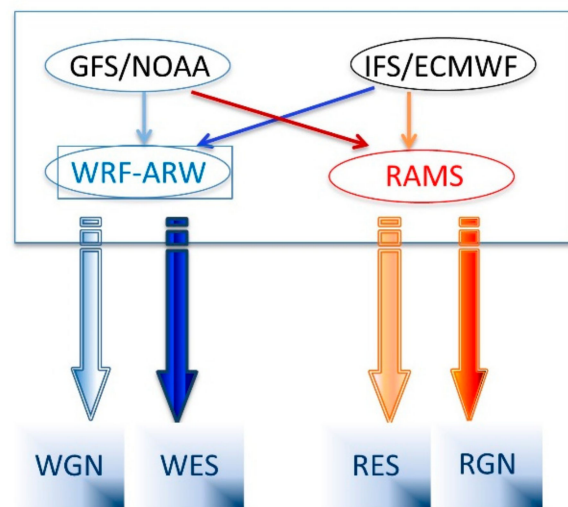


**Figure 3.** Scheme of the weather forecast obtained from four different model chains.

### 2.2.2. Satellite Data

Many authors agree on the benefit of using meteorological satellite information for the intra-day horizon of the PV power forecast, such as Barbieri et al. [12], Carriere et al. [40], Kühnert et al. [44]. The recent work of Yu [45] showed the performance improvement for a PV power generation prediction system based on the Eidetic three-dimensional (E3D)-long short-term memory (LSTM)-E3D-LSTM-model, when the future cloud amount from satellite data is included in the model with respect to the same model without cloud information inferred from satellite.

In this study also, for the VST PV power forecast, the information on the state of the sky in terms of cloudiness has been inferred from the geostationary satellite Meteosat Second Generation (MSG), operated by the European Organization for the Exploitation of Meteorological Satellites (EUMETSAT) [46]. The Spinning Enhanced Visible and Infrared Imager (SEVIRI), on board the MSG, provides data on 12 spectral channels, observing the Earth with a repeat cycle of 15 min and a spatial resolution of 3 km at the sub-satellite point for 11 channels, while a finer resolution of 1 km is available for the high-resolution visible channel, covering the range of wavelength 0.6–0.9  $\mu\text{m}$ . Through the package CloudType of the free software SAFGEO issued by the European Organization of Meteorological Satellites (EUMETSAT), represented by the Agencia Estatal De Meteorologia (AEMET), Madrid, Spain [47], the satellite images in the different channels have been analyzed and elaborated in order to classify each satellite pixel according to a particular type of cloudiness.

With this software, the nearest pixel to each PV plant has been classified, every fifteen minutes, according to the list presented in Table 2.

On the basis of the cloudiness and considering the relative position of the sun with respect to the satellite pixel at each time, the authors have derived an estimate of the *GHI* on the ground by means of a polynomial regression [48].

*GHI* has been derived from the cloud type and the Solar Zenith Angle (*SZA*) by means of the general formulation:

$$GHISat = \sum_{i=1}^3 a_{i,CT} * (\cos(SZA))^i \quad (1)$$

where the coefficients  $a_{i,CT}$  are cloud type dependent.

The estimation of the *GHI*, obtained from satellite data, has provided an input of the VST model—hereinafter referred to *GHI-Sat*.

In practice, for each time-horizon of the VST range, the predictor concerning *GHI* has been calculated according to these steps:

1. Attribution of the cloud type on the closest satellite pixel to the plant, using the latest available satellite data.
2. Calculation of the *SZA* on the site for the next horizons (+15 min, +30 min etc.)

Application of the abovementioned polynomial regression (Equation (1)) to derive the *GHI* in the future, assuming a persistence of the cloudiness and using the *SZA* at the time the forecast applies. In presence of cloudiness with rapid variations both in shape and in physical properties, the accuracy of this *GHI* forecast can rapidly worsen with increasing horizons, but it supplies a valuable update of the *NWP* forecast of the *GHI* by the way. It has been in fact proved by Dambreville et al. [49] that satellite-based methods outperform *NWP* forecast in the range of horizons +30 min +6 h with regard to *GHI* estimation.

Meteorological satellite data, besides for estimating the *GHI* in input at the *VST* model, have been used to characterize the weather conditions in correspondence of the installations in terms of cloudiness. By analyzing the cloudiness distributions on each plant, some considerations on the influence of weather conditions on the performance of the methods have arisen, as discussed both in Section 3 and in Appendix A.

**Table 2.** Cloud type classification of the SAFGEO software.

Class	Cloud Type Category
1	Cloud-free land
2	Cloud-free sea
3	Snow over land
4	Sea ice
5	Very low and cumuliform clouds
6	Very low and stratiform clouds
7	Low and cumuliform clouds
8	Low and stratiform clouds
9	Medium and cumuliform clouds
10	Medium and stratiform clouds
11	High opaque and cumuliform clouds
12	High opaque and stratiform clouds
13	Very high opaque and cumuliform clouds
14	Very high opaque and stratiform clouds
15	High semi-transparent thin clouds
16	High semi-transparent meanly thick clouds
17	High semi-transparent thick clouds
18	High semi-transparent above low or medium clouds
19	Fractional clouds (sub-pixel water clouds)

### 2.3. PV Power Forecasting Methods

The multistep PV power forecasting has been achieved through two consecutive steps:

1. Carrying out the short-term PV power forecast for the next three days with a time resolution of fifteen minutes. This forecast was performed once a day, at 12 UTC.
2. Carrying out the very-short-term power forecast every fifteen minutes, with validity up to three hours ahead.

A scheme of the process is reported in Figure 4:

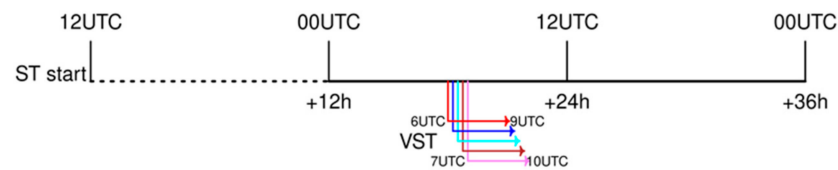


**Figure 4.** Temporal scheme representing the overlapping between the ST and the VST forecasting.

### 2.3.1. Short Term Forecast

The short-term forecast has been performed with a temporal horizon of three days and a time resolution of fifteen minutes. It has been based on a multimodel approach, both in relation to the weather information and with respect to the statistical technique used to convert weather information in power forecast.

The final *ST* prediction has been obtained by first evaluating a set of single power forecasts based on the Analog Ensemble (*AnEn*) method introduced by Delle Monache et al. [50] and then applying an optimization procedure, according to the approaches proposed by Kioutsioukis et al. [51] and applied by Collino et al. [52].

The *AnEn* method looks for a set of past events when some prescribed variables had assumed values close to those expected in the current forecast. For this study, the variables used to find similar past events were the weather variables affecting PV power production, derived from the *NWP* models mentioned in Section 2.2.1. The power measurements recorded in the past in correspondence of those “analogues” events have been used to create a probability distribution function of forecasted power. It is worth pointing out that the weather forecasts are only used to identify past moments for which the particular *NWP* model had provided a forecast similar to the current one, without actually entering into the production calculation process. The assumption is that the behavior of the *NWP* model does not change over time (the software is the same with the same parametrizations). By using a past period with power measurements and corresponding *NWP* forecast, it is safe to assume that, by comparing the current weather forecast with many past ones, it is possible to identify past power measurements that are presumably close to the ones we are going to predict. This condition is valid if the past period for finding similar events is long enough to ensure that most of the typical local weather conditions have occurred in the site where the plant is installed. In our case, a period of 29 months, from July 2016 to November 2018, has been used to identify the similar events.

From this set of past productions, it is possible to build a *pdf* from which to calculate average and median. The *pdf* is made up by managing an ensemble of past measurements, which naturally carry all the characteristics of the solar installation. In this way, some features, e.g., tilt, exposition or presence of azimuthal tracker and so on, are automatically taken into account. It is important to note that, because this *pdf* may not be normal, average and median may differ greatly from each other.

In this study, the predictors adopted to find the similar past events were: the astronomical solar angles, i.e., solar elevation (*ELEV*) and azimuth (*AZI*), the three solar irradiation components (*GHI*, *DHI* and *DNI*), the panel temperature (*TPAN*), the total precipitable water content within the vertical column of atmosphere above the solar plant (*PWC*), the relative humidity at 2 m (*RHU*), and the wind speed at 10 m above the ground (*WS*).

The PV panel temperature was evaluated by means of the formulation reported in Equation (2), derived by Skoplaki et al. [53]:

$$TPAN = T_{2m} + \frac{NOCT - 20^\circ}{800} GTI \quad (2)$$

where  $T_{2m}$  is the air temperature at 2 m above ground, *GTI* the global tilted irradiation, and *NOCT* the Nominal Operating Cell Temperature proper to the module type, defined as the temperature reached by open circuited cells in a module under standard conditions.

A preliminary analysis to identify suitable variables to be used to assess similarities was carried out by analyzing the correlograms between possible features and power

measurements. This analysis was performed for all PV plants, using power measurements and corresponding weather forecasts obtained from the four *NWP* models for one year (November 2018 to October 2019).

Figure 5a shows the correlograms, relative to plant P1, among the *AnEn* input variables, predicted by the *NWP WES*, and the production, while Figure 5b shows the highest or lowest relationships between POWER and the variables predicted by the four *NWP* for all the PV plants. In addition to the numeric values, the correlogram underlines stronger relationships by means of greater dimension of the circles and with warm colors, while small circles with cool colors represent lower correlation.

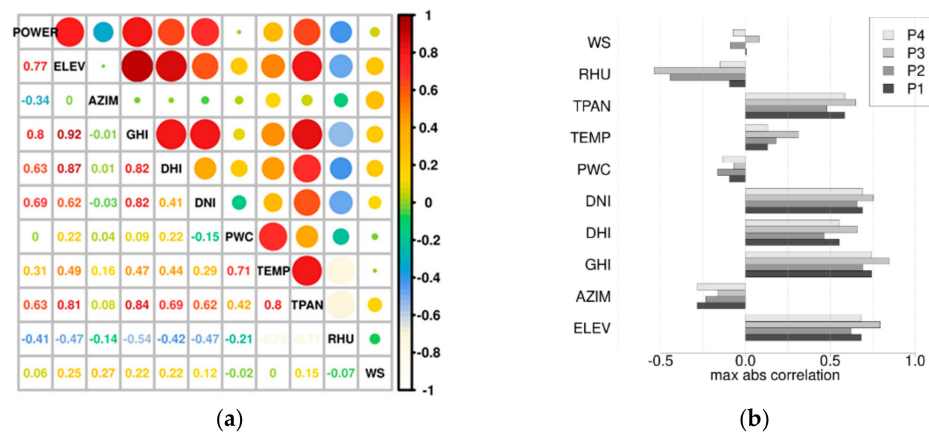


**Figure 5.** (a) Relationships between power production (POWER) and some weather variables provided by the *NWP* model *WES*, for the plant P1. (b) Maximum or minimum (over the four *NWP* models) correlation between measured production and weather variables in correspondence of the four plants.

It is interesting to observe the high correlation of the panel temperature with power, and the very low relevance of precipitable water content and wind speed. Since *TEMP* is less relevant than *TPAN*, air temperature was not used as a predictor, also to avoid redundancies and over-weighting the temperature contribution in the selection of the similar cases. Regarding *PWC*, it is important to be aware that the cloud cover used in the radiative transfer models within the *NWP* models could be significantly different from the one obtained as output of the *NWP*, because it is generally derived from independent schemes (radiative transfer models usually require knowledge of the cloud optical depth provided by *NWP*'s microphysics, whilst most cloud cover schemes are based on columnar *RHU* functions). For this reason, *PWC* was also included in the list of *AnEn* features. Wind intensity was also considered, despite its low relationship with power, with a view to creating a generalized model and taking into account that wind has a significant rule in heat dissipation and could affect module efficiency, especially in locations with variability in wind regimes and for outdoor installations.

All these weather variables have been provided by the regional models mentioned in Section 2.2.1. The two regional models (*WRF* and *RAMS*), driven by the initial and boundary conditions supplied by two different global *NWP* (*IFS* and *GFS*), have made it possible to obtain four different *NWP* configuration, named *RES*, *RGN*, *WES*, *WGN*, as shown in Figure 4. Since the outputs of these models have an hourly time step to save calculation resources, the weather time series have been linearly interpolated with a resolution of 15 min, in accordance with the time resolution of the power measurements.

As mentioned above, *AnEn* looks for similar past events by minimizing the distance between the current set of predictors and the past ones. The metric adopted for evaluating

the distance between the current vector of predictors and the past forecasts is the one reported in Equation (3), named absolute distance in the following:

$$d_{Abs}(t, t') = \sum_{v=1}^{N_v} \frac{w_v}{\sigma_v} |F_{v,t} - A_{v,t'}| \quad (3)$$

where  $v$  represents each variable of the set of  $N_v$  predictors,  $F_{v,t}$  the  $v$ -th component of the array of the current forecast for the forecast horizon  $t$ , and  $A_{v,t'}$  the  $v$ -th component of the past forecasts relative to the same temporal horizon of  $F_{v,t}$ . Each variable used to evaluate the distance has been previously normalized using the standard variation  $\sigma_v$  of each variable inside the training period considered. For this study, the training period ran from July 2016 to November 2018, and the test period from November 2018 to November 2019. The training and test periods are chosen large enough to avoid monthly calendar effect, whilst yearly effects may occur due to climatological anomalies. According to the formulation reported in Equation (3), it is also possible to set different weights for each variable through  $w_v$ . Compared to the *AnEn* introduced by Delle Monache et al. [50], the *AnEn* implemented in this study has some different features, such as the fact that the metric compares only the predictors at the same temporal horizons, and the absolute distance is adopted instead of the Euclidean one. Furthermore, in the selection of similar past events a constraint has been imposed on the astronomical angles, considering only the events for which the past and the current zenith angle differed for less than 10 degrees, and the azimuths for less than 20 degrees, in order to guarantee similar solar positions.

For each plant, at each *NWP* forecasting run, different *AnEn* setups have been performed, by varying the configuration of the *AnEn* according to the following criteria, summarized in Table 3:

- The inputs used by the *AnEn*:

There were used weather forecasts provided by a single *NWP* model of the four described in Section 2.2.1 (*RES*, *RGN*, *WES*, *WGN*), or by all of them simultaneously (*MM*). In the latter case the meteorological input was made of 28 weather variables (the 7 meteorological variables listed above and provided by the 4 *NWP* models).

- The application of a pre-processing on the predictors by means of:

Principal Component Analysis (*PCA*). Instead of using the forecasted weather variables, the distance was calculated using the  $N_{PCA}$  principal components selected on the basis of the explanation of the 95% of the variance. *PCA* was only used to create additional ensemble members, again based on Analog Ensemble. Basically, the aim was to reduce the cardinality of the input set, especially when all four *NWP* models, i.e., 28 weather variables, were used, to avoid curse of dimensionality problems.

- The number of elements of the *pdf*:

The metric (Equation (3)) allows to identify the  $N_{pdf}$  past events more similar to the current one. The number  $N_{pdf}$  is another free parameter, usually set to the square root of the length of the training dataset. Beside the value suggested by the thumb rule ( $N_{pdf} = 21$ ), the case  $N_{pdf} = 31$  was also used.

- Application of some weights to the predictors:

Some configurations (*WI* and *WJ*) considered variable-dependent weights, obtained after a sensitivity study, whilst in the other cases each variable was normalised only for its standard deviation.

According to the presented criteria, by applying the Equation (3) it has been possible to select an ensemble of past  $N_{pdf}$  power measurements with which to build different probability distribution functions of the expected production. From these *pdfs*, the average, the median and the major percentiles have been computed for each of the configurations summarized in Table 3.

**Table 3.** List of the *AnEn* configurations.

Config	Configuration Parameters			NWP				
	$N_{pdf}$	$w_v$	PCA	RES (RAMS + IFS)	RGN (RAMS + GFS)	WES (WRF + IFS)	WGN (WRF + GFS)	MM
WI	21	yes	no	IREWI	IRGWI	IWEWI	IWGWI	IMMWI
WJ	31	yes	no	IREWJ	IRGWJ	IWEWJ	IWGWJ	IMMWJ
WM	21	no	no	IREWM	IRGWM	IWEWM	IWGWM	IMMWM
WN	31	no	no	IREWN	IRGWN	IWEWN	IWGWN	IMMWN
PM	21	no	yes	IREPM	IRGPM	IWEPM	IWGPM	IMMPM
PN	31	no	yes	IREPN	IRGPN	IWEPN	IWGPN	IMMPN

Once the configured forecasts have been performed, an optimization procedure has been applied to their ensemble  $E$ , based on the minimization of the following error, described by Kioutsioukis [51]:

$$MSE(\bar{f}) = \overline{bias}^2 + \frac{1}{M} \overline{varE} + \left(1 - \frac{1}{M}\right) \overline{covE} \quad (4)$$

which states that the mean squared error ( $MSE$ ) of an ensemble ( $E$ ) of single forecasts is made up of three contributes: bias, variance and covariance of the ensemble composed of  $M$  members. In order to optimize the ensemble, both the mean and the median of each  $pdf$  have been used in Equation (4), for a total of 60 members. Since the members of the ensemble were correlated to each other, the optimized forecast (solution of Equation (4)) has been written as a weighted average of the  $M$  members:

$$\bar{f} = \sum_{k=1}^M a_k f_k \frac{\underline{K}^{-1} \underline{u}}{(\underline{K}^{-1} \underline{u}, \underline{u})} \cdot f \quad (5)$$

where  $\bar{f}$  is the ensemble average,  $\underline{K}$  the ensemble's correlation matrix,  $f_k$  the  $k$ -th member of the ensemble, and  $\underline{u}$  is a vector of ones of length  $M$ . Following this approach, the weights  $a_k$  may not be definite positive, allowing some sort of compensation between different ensemble members, i.e. between different *AnEn* configurations and/or *NWP* outputs (positive weights are obtained only if the ensemble members are uncorrelated).

The advantages of applying the ensemble optimization method are discussed in Section 3.

### 2.3.2. Very Short-Term Forecast

The forecast for the following three hours, with a time resolution of fifteen minutes has been based on an Auto-Regressive Integrated Moving Average Model with exogenous input (ARIMAX). ARIMAX is a multivariate version of the time series method ARIMA and its use in PV power forecasting has been explored by only a few authors so far, such as Zhou et al. [13], Bacher et al. [17], Perez-Mora et al. [18]. ARIMA method is a generalization of ARMA modelling with the advantage of handling nonstationary time series. It was introduced by Box and Jenkins [54]. ARIMA is made up of three elements: autoregression (AR), integration (I) and moving average (MA). It is characterized by three parameters ( $p, d, q$ ), where  $p$  is the number of time lags of the autoregressive model,  $d$  is the degree of differencing and  $q$  is the order of the moving-average model.

In the past only observed or predicted *GHI*, air temperature, or PV panel temperature were considered as input of ARIMAX devoted to forecast PV power. Yang in [55] claimed the lack of weather information on time series models developed so far. In this study an innovative autoregressive method has been carried out, focusing on the use of new

exogenous inputs and exploring the usefulness of introducing irradiance data derived from satellite and power forecasts obtained from independent methods as predictors.

The exogenous variables selected as input of the very-short-term forecasting are:

- *GHI* from satellite data (*GHI-Sat*)
- *GHI* from satellite data (*GHI-Sat*) Smart Power Persistence (*SP*)
- Short-Term PV power Forecasting (*ST*)

The predictor *GHI-Sat* has been already described in Section 2.2.2.

*SP* is a smart power persistence, established by considering the evolution of the solar orbit.

The persistence model (or naïve model) supposes that conditions at time  $t$  will persist into the time period  $t + i$  and, for this reason, the forecast for the time  $t + i$  corresponds to the power registered at the time  $t$ :  $P_{t+i} = P_t$ , where  $i$  represents the time lag in the future, such as minutes, hours, or even days. Solar production strongly depends on the elevation of the Sun and therefore it is possible to calculate a smart power persistence in the future, normalizing the persistence with the variations of the solar zenith angle on the plant and taking into account also the dependence of the extra-terrestrial radiation with time.

The formulation of the *SP* is reported in Equation (6):

$$P_{t+i} = P_t \frac{I_{t+i} * \cos \theta_{t+i}}{I_t \cos \theta_t} \quad (6)$$

where  $P_{t+i}$  is the *SP*, that is the forecasted production at the step  $t+i$ ,  $\theta$  is the solar zenith angle and  $I_t$  is the solar constant corrected with the Sun-Earth distance at each time  $t$ .

The predictor *ST* consists of the PV power forecast issued the day before for each time frame corresponding to the very-short-term horizons. For example, as shown in Figure 4, the nowcasting starting at 6 UTC for the next hour (7 UTC.), will use, as predictor, the *ST* issued the previous day at 12 UTC with time horizon +19 h, that is the power expected at 7 UTC.

The selection of the exogeneous input derives, in part, from previous studies, performed by the authors, devoted to quantify the performance of the ARIMAX model to varying input, in part analyzing the Spearman correlation between possible predictors and power measurements. Different authors, including Ahmed et al. [9] and Yang et al. [55], assert that the real challenge in PV power forecasting is the design of the model with the optimum number of inputs, avoiding irrelevant predictors, that could lead to undesirable increase of prediction variance.

The relationships among the variables have been studied for all the plants, considering one year of measurements every fifteen minutes and the corresponding possible predictors. The initial series of predictors taken into account consisted of  $\cos(\text{SZA})$ , air temperature, panel temperature, *GHI* derived from *NWP* (*GHI-NWP*), *GHI* derived from satellite, *SP* and *ST*.

The relationships were found to slightly vary from place to place and according to the forecast horizon, but *GHI-Sat*, *SP* and *ST* were found to be the variables most related with power measurements. In Figure 6 a graphical display of the correlation matrix is presented for the plant P1. In the graph, Figure 6a is the correlogram calculated considering the exogenous input at the time horizon of 15 min, while Figure 6b refers to the 180 min forecast. The relationships among the variables are always positive.

Considering the relationships shown in Figure 6, it is possible to note that, in addition to *GHI-Sat*, *SP* and *ST*, also *GHI-NWP* and  $\cos(\text{SZA})$  present high relationships with power, but they are mutually related also with *ST* of which they are inputs. Therefore, in order to avoid redundancy, these two variables have not been used as predictors in the VST.

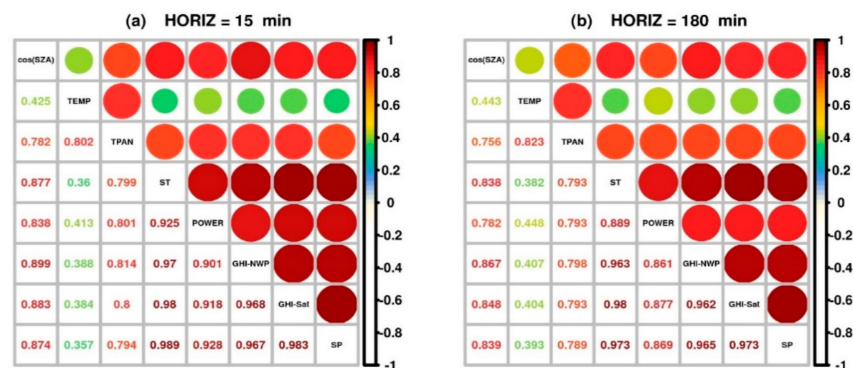


**Figure 6.** Correlogram between possible predictors and power measurements related to the forecasting horizon of 15 min (a) and 180 min (b) for the plant P1.

ARIMAX model has been implemented using the function `auto.arima` of the package `forecast v8.13` of R developed by Hyndman et al. [56], applying a pre-processing to the input, in order to normalize each variable in the range 0–1. This function builds and evaluates different ARIMAX models and finally selects the best one on the basis of different possible criteria (in this study the Akaike’s Information Criterion has been used). The selection of the “optimum” ARIMAX has been performed at each run, using the last three weeks of historical power in order to create and test different possible ARIMAX and select the best one. Due to the fact that autoregressive models run very fast, for the VST it has been possible to derive every fifteen minutes an updated model, adapted to the recent behavior of the plant.

#### 2.4. Performance Metrics

The developed models have been evaluated considering a wide range of performance metrics: normalized Mean Bias Error ( $nMBE$ ), normalized Mean Absolute Error ( $nMAE$ ), normalized Root Mean Square Error ( $nRMSE$ ), Forecast Skill with respect to MAE ( $FSMAE$ ), Forecast Skill with respect to RMSE ( $FSRMSE$ ).

The normalization of the errors has been performed with respect to the maximum value of measured power. It is common that the PV plant output does not achieve the nominal power and therefore the normalization with respect to the maximum registered, instead of the nominal power, is more useful in order to quantify the errors in operational conditions.

In Equations (7)–(11) the definitions of the error metrics are reported, considering that  $W^{fore}$ ,  $W^{obse}$ ,  $W^{Mobse}$ ,  $N$ ,  $mod$ ,  $ref$  represent the forecasted power at each time point, the corresponding measured power, the maximum observed power, the sample size, the forecasting model and the reference model respectively.

$$nMBE = \frac{\frac{1}{N} \sum_{k=1}^N (W_k^{fore} - W_k^{obse})}{W^{Mobse}} \times 100 \quad (7)$$

$$nMAE = \frac{\frac{1}{N} \sum_{k=1}^N |W_k^{fore} - W_k^{obse}|}{W^{Mobse}} \times 100 \quad (8)$$

$$nRMSE = \left( \sqrt{\frac{1}{N} \sum_{k=1}^N (W_k^{fore} - W_k^{obse})^2} \right) \times \frac{100}{W^{Mobse}} \quad (9)$$

$$FSMAE = 1 - \frac{nMAE_{mod}}{nMAE_{ref}} \times 100 \quad (10)$$

$$FSRMSE = 1 - \frac{nRMSE_{mod}}{nRMSE_{ref}} \times 100 \quad (11)$$

Regarding error metrics, the authors have decided to evaluate the forecasting skill, both with respect to  $nMAE$  and  $nRMSE$ . At present, in fact, there is no consensus about the preference for MAE or RMSE in determining the forecasting performance (see Cort et al. [57], Botchkarev et al. [58], Choi et al. [59]). It is important to be aware that each error metric describes a particular aspect of the model error characteristics. For this reason, it is useful to consider different types of metrics, in order to better describe the model performance according to various aspects, such as systematic over/under estimation, magnitude of the errors in absolute and quantification of large errors.

The errors have been calculated considering only day-time data and for each time horizon, to compare the usefulness of the methods varying the forecasting horizon.

The reference model used to calculate skill scores both for the ST and the VST forecasting is the smart power persistence, described in Section 2.3.2.

For a better understanding of the influence of ST errors to VST forecasts, the Mean Absolute Error  $MAE = \frac{1}{N} \sum_{k=1}^N (W_k^{fore} - W_k^{obse})$  obtained using ST and VST forecasts have been analyzed in order to calculate the *real-time* performance of the ST and VST during the whole test period.

In practice, we have considered different prediction horizons of the VST, from 60 min up to 150 min, although the comparison is mostly useful for the 60- and 90-min horizons. For each plant, for evaluating the real-time errors for each day  $d$  belonging to the test period, the starting times  $t_{start} \in [t_{sunrise} + K, t_{sunset} - K]$  ( $t_{sunrise}$  and  $t_{sunset}$  are the time of sunrise and sunset respectively) and different forecast horizons  $K \in \{60, 90, 120, 150\}$  have been considered. The forecasted ST and VST power production can be formally expressed as in Equations (12) and (13) respectively:

$$P^{ST}(d-1; 12 + t_{start}; f_m) \quad (12)$$

$$P^{VST}(d; t_{start}; f_m) \quad (13)$$

where the ST run starting at 12 UTC of the day before the current one is signed as  $(d-1)$ , and the forecasts  $f_m \in F_K$ ,  $F_K = \{15, 30, \dots, K\}$  with steps of 15 min. According to the same notation, the measured power production of the plant, relative to the hour  $(t_{start} + f_m)$  of the day  $d$ , is  $P^{meas}(d; t_{start} + f_m)$ . The *real-time* forecast error is evaluated at each starting time by averaging the absolute errors for all the forecasts belonging to the set  $F_K$ . In particular, Equation (14) relates to the ST forecast and Equation (15) to the VST forecast.

$$E_K^{ST}(d; t_{start}) = \frac{1}{(K/15)} \sum_{f_m \in F_K} \left| P^{ST}(d-1; 12 + t_{start}; f_m) - P^{meas}(d; t_{start} + f_m) \right| \quad (14)$$

$$E_K^{VST}(d; t_{start}) = \frac{1}{(K/15)} \sum_{f_m \in F_K} \left| P^{VST}(d; t_{start}; f_m) - P^{meas}(d; t_{start} + f_m) \right| \quad (15)$$

The range of  $E_K^{ST}$  is the interval  $[0, \Delta_K]$ , which is divided into  $n_\delta$  (set equal to 300 in this study) subintervals of equal width.

To guarantee the synchronization of the errors provided by ST and VST, data are partitioned in a set of disjoint and adjacent sets  $\{A_r\}$  defined as reported in Equation (16):

$$A_r = \left\{ (d; t_{start}) \left| \frac{(r-1)\Delta_K}{n_\delta} \leq E_K^{ST} < \frac{r\Delta_K}{n_\delta} \wedge r \in [1, n_\delta] \right. \right\} \quad (16)$$

The partitioning is performed with respect to ST errors belonging to the whole test period. This means that the set  $A_{\hat{r}}$  contains the time labels of the events for which the ST errors lie in an interval of width  $\Delta_K/n_\delta$  starting at  $(\hat{r}-1)\Delta_K/n_\delta$ . Naming  $\varepsilon_{\hat{r}}^{ST}$  the centre

of this interval, the total run-time error (expressed in power units) for each subinterval is defined as:

$$Q^{ST} = \sum_{(d;t_{start}) \in A_r} E_K^{ST}(d;t_{start}); Q^{VST} = \sum_{(d;t_{start}) \in A_r} E_K^{VST}(d;t_{start}) \quad (17)$$

and the corresponding cumulative quantities as:

$$C_r^{ST}(\varepsilon_r^{ST}) = \sum_{k=1}^r Q_k^{ST}(\varepsilon_k^{ST}); C_r^{VST}(\varepsilon_r^{ST}) = \sum_{k=1}^r Q_k^{VST}(\varepsilon_k^{ST}) \quad (18)$$

The analysis of the errors is discussed in Section 3.

### 3. Results

In this work, both the *ST* and *VST* forecasting models have been applied to forecast the PV production at four different Italian sites, during the period November 2018–November 2019. The PV plants and the used dataset have been described in Section 2.1, while the analyzed error metrics have been presented in Section 2.4. All the tested methods have been compared with the smart power persistence, introduced in Equation (6) and used as reference.

Firstly, the general ability of the *ST* in predicting PV power, up to three days ahead has been considered.

As described in Section 2.3.1, the optimized short-term forecast has been obtained by solving Equation (5), using 60 member ensembles made up of the average and medians provided by the *AnEn* pdfs.

In Figure 7 the nRMSE vs. nMAE for each ensemble member is shown for the plants P2 and P4 and for the first and third forecasting day, respectively. The most relevant considerations that can be made are that medians get larger errors than averages, the *MM* forecasts—corresponding to the red circles and crosses at the lower ends of the ellipses—always achieve better results than any single *NWP*, the pre-processing with PCA generally performs worst, and finally the optimized *ST* always obtains smaller errors than any single *AnEn* forecast.

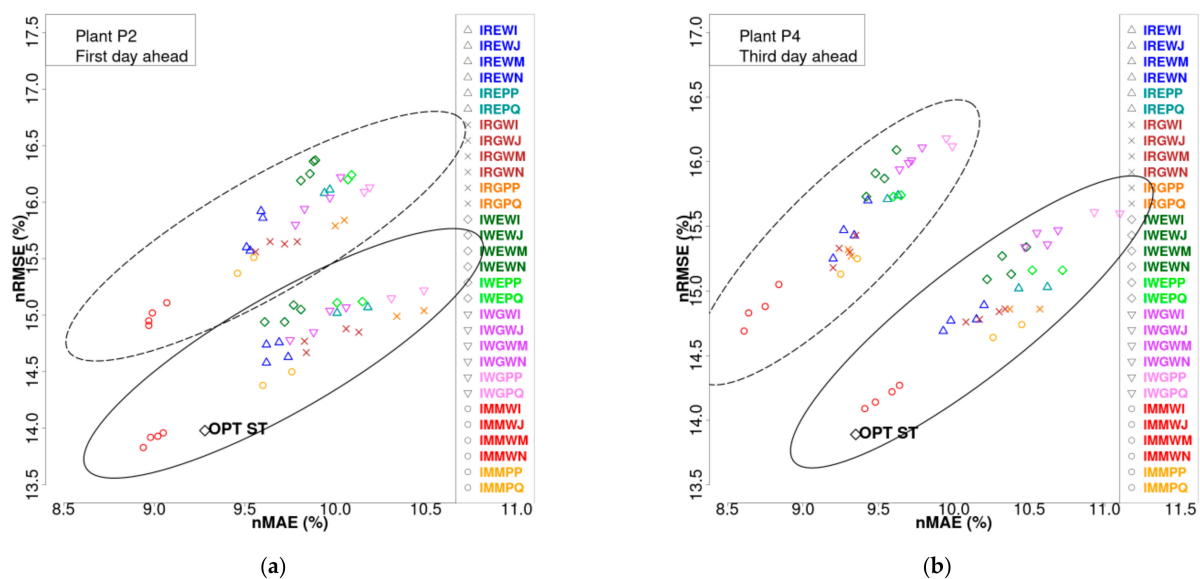


**Figure 7.** Normalised root mean square error (nRMSE) vs. relative Mean Absolute Error (nMAE) of the *M* members of the ensemble for plant P2 (forecasts for the first day ahead) (a) and plant P4 (b) (forecasts for the third day ahead). Inside the dashed ellipses there are drawn members obtained using median of *AnEn* pdf, inside the continuous ellipses those obtained using the mean of pdf. The blue rhombuses indicate the errors of the optimized power forecasts.

In Table 4 the normalized  $nMAE$ ,  $nRMSE$  and the skills ( $FSMAE$  and  $FSRMSE$  evaluated with respect to the smart power persistence  $SP$ ) of the optimized  $ST$  model are summarized. They represent the average of the errors produced in the first, second and third day of forecast during the entire verification period.

The  $nMAE$  and  $nRMSE$  of the optimized  $ST$  increase with the time horizon by about half a percentage point, moving from the first to the third day of forecasting. The better results, in terms of  $nMAE$  and  $nRMSE$  are achieved for the plant  $P4$ , probably due to its climatology, dominated by a large amount of clear sky conditions. This aspect has been investigated using satellite data in order to evaluate the general weather conditions of each site and the main findings are reported in Appendix A.

**Table 4.**  $nBIAS$ ,  $nMAE$ ,  $nRMSE$ , and SKILLS of the four PV plants. The values are the mean errors, in percentages, regarding the first (horizon of 12–36 h), the second (36–60 h), and the third (60–84 h) day ahead. The errors have been normalized with respect to the maximum measured value ( $P1_{max} = 12.44$  kW,  $P2_{max} = 15.29$  kW,  $P3_{max} = 40$  kW,  $P4_{max} = 13.94$  kW).

Forecast Horizon	P1				P2			
	$nMAE$	$nRMSE$	$FSMAE$	$FSRMSE$	$nMAE$	$nRMSE$	$FSMAE$	$FSRMSE$
First day	9.40	13.41	27.69	36.92	9.28	13.98	33.24	37.14
Second day	9.52	13.52	34.12	41.14	9.42	14.01	38.31	41.16
Third day	9.91	13.89	30.46	38.81	9.84	14.52	36.88	39.68
Forecast Horizon	P3				P4			
	$nMAE$	$nRMSE$	$FSMAE$	$FSRMSE$	$nMAE$	$nRMSE$	$FSMAE$	$FSRMSE$
First day	9.90	14.59	31.06	35.98	8.81	13.23	33.96	39.89
Second day	10.07	14.74	36.43	39.19	9.01	13.35	37.99	43.22
Third day	10.43	15.12	33.44	36.60	9.35	13.89	33.83	39.66

The  $nMAE$  and  $nRMSE$  of the optimized  $ST$  increase with the time horizon by about half a percentage point, moving from the first to the third day of forecasting. The better results in terms of  $nMAE$  and  $nRMSE$  are achieved for the plant  $P4$ , probably due to its climatology, dominated by a large amount of clear sky conditions. This aspect has been investigated using satellite data in order to evaluate the general weather conditions of each site and the main findings are reported in Appendix A.

Taking into account this behavior, it is interesting to consider the improvements achievable with the use of the optimized  $ST$  with respect to the smart persistence, evaluated using the observed power with lags of one, two, or three days before the forecast time for the first, second and third day of forecast respectively.

The forecast skill scores are larger than 30%, except for the  $FSMAE$  of  $P1$  for the first day of forecast, with varying fluctuations going from the first to the third day of forecast. The nonmonotonic increase of the skills with the forecasting horizon is due to the nonconstant increase with time of the errors for the smart power persistence.

It is important to underline the ability of the optimized  $ST$  in avoiding errors of large magnitude, because the  $FSRMSE$  scores are always greater than the  $FSMAE$  ones and exceed 40% except for the plant  $P3$ , where the best score is 39.2%.

Considering the intra-day forecast, the purpose of this work was to evaluate advantages and drawbacks of different approaches, suitable for real-time applications, with varying time frames, from 15 min up to three hours ahead. In particular, having available the optimized  $ST$  forecasting for the next day, we wanted also to figure out the forecasting horizon up to which the  $VST$  outperformed the  $ST$ , in order to identify which method was preferable to use at each forecasting horizon.

Figure 8 presents the evolution of  $nMAE$  and  $nRMSE$  with the increase of the forecasting horizon, from 15 min up to the 180 forthcoming minutes for the main methods considered in this work, such as pure and smart power persistence—calculated using the last available power measurement—ARIMAX and optimized  $ST$ .

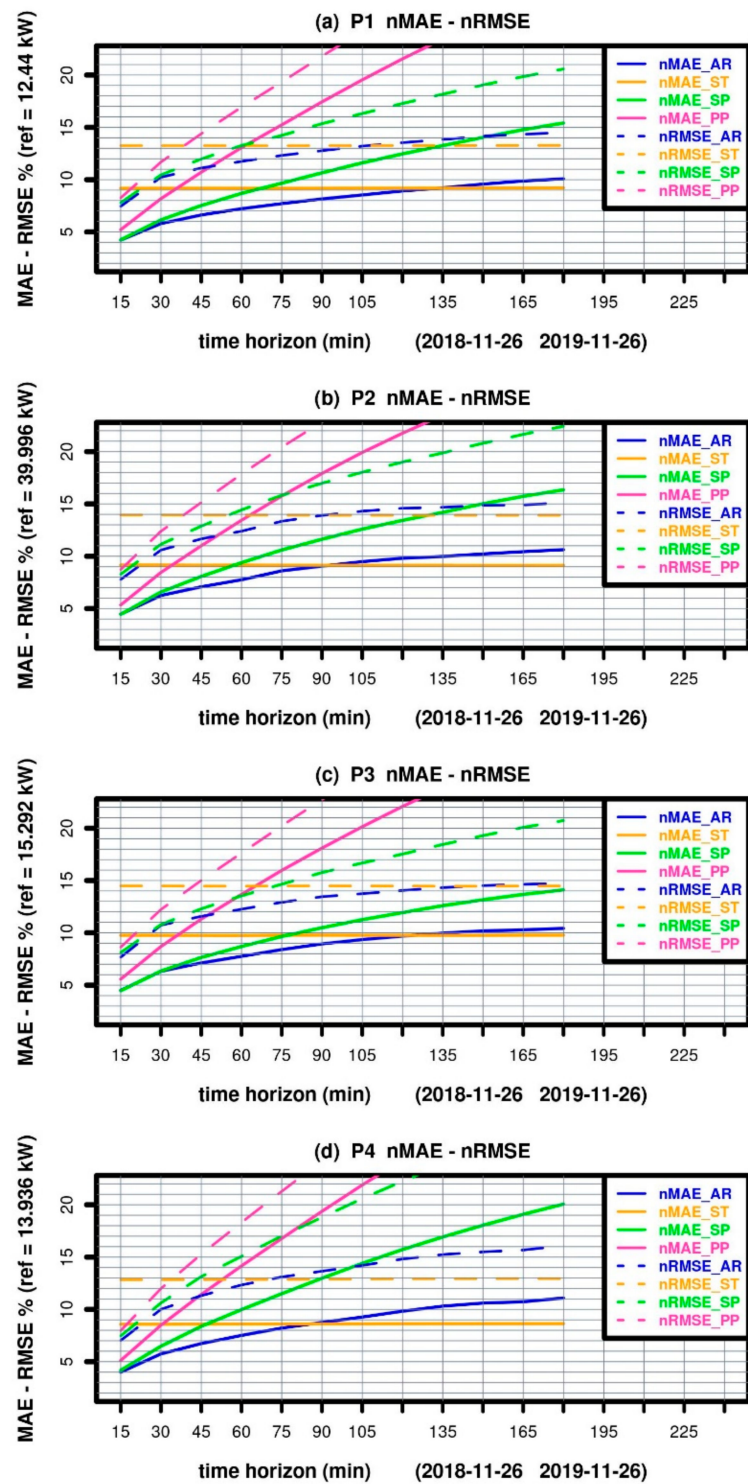


Figure 8. *nMAE* (solid) and *nRMSE* (dashed) errors as a function of the prediction horizon for ARIMAX(*AR*) in blue, optimized short-term (*ST*) forecasting in orange, smart persistence (*SP*) in green and pure persistence (*PP*) in pink, related to the plants P1 in the panel (a), P2 in (b), P3 in (c) and P4 in (d).

By analyzing the evolution of both  $nMAE$  and  $nRMSE$  in Figure 8, it is possible to note the outperformance of all the very-short-term forecasting methods ( $PP$ ,  $SP$ ,  $AR$ ) with respect to the  $ST$  for the early forecasting horizons. However, after only 30 min, the  $ST$  outperforms the  $PP$  in each site.

The smart power persistence turns out to be a satisfactory PV forecasting method at least in the first hour of forecast, with  $nMAE$  ranging from about 4% to 9% with small variations depending on the plant. In the very-short forecasting range, as the time goes on, the most beneficial system, both in terms of  $nMAE$  and  $nRMSE$ , proves to be the ARIMAX. In fact, it achieves the lowest rate of errors from the beginning up to over two hours in advance for the plants P1 and P3 and up to 90 min for the plants P2 and P4. ARIMAX starts with a  $nMAE$  around 4% and a  $nRMSE$  around 7.5% and reaches values around 10.2% of  $nMAE$  and 15% of  $nRMSE$  after three hours in P1, P2 and P3 sites, while the behavior is different for P4 plant. In this case ARIMAX gains very low errors at the first horizon, with a  $nMAE$  of 3.99% and a  $nRMSE$  of 7.0%, but, after three hours, the  $nMAE$  is one percentage point larger than the one obtained in the other plants and so for  $nRMSE$ . The reason of this evolution has been investigated through analysing the climatology of the site where the plant is installed, in terms of cloudiness, as reported in Appendix A.

By analyzing the evolution of both  $nMAE$  and  $nRMSE$  in Figure 8, it is possible to note the outperformance of all the very-short-term forecasting methods ( $PP$ ,  $SP$ ,  $AR$ ) with respect to the  $ST$  for the early forecasting horizons. However, after only 30 min, the  $ST$  outperforms the  $PP$  in each site. The smart power persistence turns out to be a satisfactory PV forecasting method at least in the first hour of forecast, with  $nMAE$  ranging from about 4% to 9% with small variations depending on the plant. In the very-short forecasting range, as the time goes on, the most beneficial system, both in terms of  $nMAE$  and  $nRMSE$ , proves to be the ARIMAX. In fact, it achieves the lowest rate of errors from the beginning up to over two hours in advance for the plants P1 and P3 and up to 90 min for the plants P2 and P4. ARIMAX starts with a  $nMAE$  around 4% and a  $nRMSE$  around 7.5% and reaches values around 10.2% of  $nMAE$  and 15% of  $nRMSE$  after three hours in P1, P2 and P3 sites, while the behavior is different for P4 plant. In this case ARIMAX gains very low errors at the first horizon, with a  $nMAE$  of 3.99% and a  $nRMSE$  of 7.0%, but, after three hours, the  $nMAE$  is one percentage point larger than the one obtained in the other plants and so for  $nRMSE$ . The reason of this evolution has been investigated through analysing the climatology of the site where the plant is installed, in terms of cloudiness, as reported in Appendix A.

As far as concern the presence of systematic over/underestimation from the various very-short-term methods, Tables 5–8 present the relative  $nBIAS$  for each plant in function of the time horizon.  $PP$  shows a general underestimation, with increasing values as the forecasting horizon grows, except for the plant P1, where a slight overestimation is experienced. Instead,  $SP$  shows different behaviors at the various locations. An important overestimation, with growing values as the lead-time increases, is registered for the plants P1 and P4, while lower values are obtained for P2. On the contrary, at the P3 site, the  $nBIAS$  is very low, with a slight underestimation for lead-times beyond one hour. The  $ST$  has positive  $nBIAS$  for plants P2 and P3, while there is a slight underestimation for P1 and P4.

In addition to systematic errors, both producers and system operators are interested in assessing how much a method is beneficial with respect to another one, in absolute terms, and to quantify the presence or absence of large errors. In order to make this comparison easier, the skill of the forecast with respect to the  $SP$  system, used as benchmark, has been calculated according to the Equations (10) and (11). It is important to note that, despite its simplicity,  $SP$  is a powerful prediction system. Its reliability can be verified by comparing its performance with respect to the performance of the  $PP$ , analyzing in details the progress of the errors in Figure 8. Already at the first lead time (+15 min),  $SP$  gets a  $nMAE$  one percentage point lower than  $PP$  and the gap widens more and more with increasing forecasting horizons. The authors have also implemented an ARIMA forecasting tool for each plant. ARIMA is often used as baseline for the VST, but it got worst performances with respect to  $SP$ , therefore the authors have set to using  $SP$  as a

robust baseline to deal with. Tables 5–8 report the *FSMAE* and the *FSRMSE* for each plant according to the lead-time.

As far as *FSMAE* concerns, with ARIMAX, the skill is always positive, except for the plants P2 and P3, where it is slightly negative at the first horizon, confirming the validity of the *SP* as a useful forecasting method for the first horizons.

The *FSMAE* of ARIMAX grows as the time goes on. The greatest benefit is registered for plant P4, with a value of 44.7% at the 180 min time horizon. This result must be nevertheless compared with *ST*. Even if *FSMAE* of *ST* is negative, in general, during the first hour, it exceeds ARIMAX beyond 120 min for the plants P1 and P3 and over 75 min for sites P2 and P4. By considering the *FSRMSE*, the behavior is different on the four plants. The skill of ARIMAX is always positive and so for *ST* after, at least, one hour of forecast.

Regarding the comparison between ARIMAX and *ST*, *ST* outperforms ARIMAX beyond 60 min of forecast at P4, over 90 min at P2, beyond 105 min at P1 and over 135 min at P3.

These variations suggest that it is important to analyze several error indexes to obtain an overall view of the characteristics of a PV power forecasting method.

In this work, a reliable *VST* forecasting, by using a very fast method, suitable for real-time operation, has been achieved by means of an ARIMAX that uses the output of the *ST* as explanatory variable, together with the *GHI* from satellite and the *SP*.

**Table 5.** Normalised BIAS and forecast skill related to MAE-FSMAE and RMSE-FSRMSE for plant P1 from 15 min up to three hours ahead.

LAG	NUM	nBIAS_AR	nBIAS_ST	nBIAS_SP	nBIAS_PP	FSMAE_AR	FSMAE_ST	FSMAE_PP	FSRMSE_AR	FSRMSE_ST	FSRMSE_PP
15	15049	0.23	-0.68	0.60	0.22	0.48	-115.88	-22.73	4.43	-69.96	-5.93
30	15035	0.14	-0.68	1.19	0.47	5.68	-49.25	-33.01	2.08	-26.84	-11.81
45	15037	0.24	-0.69	1.71	0.72	12.00	-21.99	-42.27	7.21	-10.66	-20.15
60	15036	0.30	-0.68	2.22	1.03	16.86	-5.71	-50.32	11.46	0.11	-27.66
75	15054	0.73	-0.68	2.71	1.20	20.22	5.03	-57.69	13.44	6.91	-35.88
90	15044	0.83	-0.67	3.19	1.28	23.41	13.79	-63.69	16.84	13.69	-41.99
105	15035	0.95	-0.68	3.63	1.25	26.45	20.83	-68.33	19.06	18.76	-48.26
120	15039	0.96	-0.68	4.06	1.13	28.43	26.26	-72.87	21.66	23.26	-53.44
135	15034	1.04	-0.68	4.49	0.89	30.49	30.66	-76.81	23.84	27.00	-58.10
150	15029	0.94	-0.69	4.90	0.55	31.81	34.46	-80.07	25.64	30.35	-61.84
165	15027	0.96	-0.69	5.29	0.11	33.17	37.70	-82.81	27.81	33.14	-65.62
180	15029	1.02	-0.69	5.69	-0.43	34.60	40.25	-85.78	29.47	35.48	-68.98

**Table 6.** Normalized BIAS and forecast skill related to MAE-FSMAE and RMSE-FSRMSE for plant P2 from 15 min up to three hours ahead.

LAG	NUM	nBIAS_AR	nBIAS_ST	nBIAS_SP	nBIAS_PP	FSMAE_AR	FSMAE_ST	FSMAE_PP	FSRMSE_AR	FSRMSE_ST	FSRMSE_PP
15	12916	0.20	2.28	0.36	0.00	-0.45	-105.83	-20.13	5.99	-68.43	-5.45
30	12904	0.14	2.29	0.65	-0.01	5.06	-39.09	-28.43	5.01	-25.01	-11.09
45	12912	0.31	2.29	0.88	-0.04	12.25	-13.34	-36.37	9.47	-8.18	-17.55
60	12911	0.37	2.28	1.06	-0.12	17.39	2.49	-43.21	14.08	3.38	-23.70
75	12917	0.69	2.28	1.19	-0.25	18.81	13.75	-48.70	15.69	11.99	-29.10
90	12919	0.83	2.28	1.29	-0.46	22.10	21.44	-54.07	18.09	18.00	-34.52
105	12917	0.85	2.26	1.34	-0.79	24.68	27.48	-58.20	20.63	22.80	-39.21
120	12908	0.81	2.26	1.41	-1.19	26.94	31.99	-62.05	23.24	26.75	-43.37
135	12906	0.88	2.27	1.47	-1.66	29.69	35.66	-65.42	26.15	29.98	-47.14
150	12913	0.90	2.26	1.53	-2.21	31.93	39.22	-67.36	28.56	33.11	-49.87
165	12911	0.80	2.27	1.62	-2.82	33.66	41.97	-69.71	31.18	35.74	-52.48
180	12898	0.56	2.27	1.68	-3.54	35.00	44.15	-72.27	32.58	37.94	-54.89

**Table 7.** Normalized BIAS and forecast skill related to MAE-FSMAE and RMSE-FSRMSE for plant P3 from 15 min up to three hours ahead.

LAG	NUM	nBIAS_AR	nBIAS_ST	nBIAS_SP	nBIAS_PP	FSMAE_AR	FSMAE_ST	FSMAE_PP	FSRMSE_AR	FSRMSE_ST	FSRMSE_PP
15	15979	0.05	4.00	0.13	-0.04	-0.79	-118.90	-24.87	5.40	-78.65	-6.35
30	15981	-0.03	4.00	0.17	-0.11	0.34	-53.67	-36.86	0.54	-34.19	-13.32
45	15984	-0.06	4.00	0.15	-0.24	6.83	-27.62	-47.99	5.86	-17.66	-22.10
60	15988	-0.03	3.99	0.08	-0.45	10.87	-12.13	-57.28	9.45	-6.82	-30.18
75	15957	0.12	4.01	-0.02	-0.76	12.95	-1.27	-65.48	11.82	1.15	-38.10
90	15956	0.09	4.01	-0.14	-1.14	14.75	6.82	-72.60	14.65	8.10	-44.27
105	15964	0.00	4.01	-0.27	-1.60	16.90	13.26	-78.91	17.61	13.20	-50.67
120	15961	-0.02	4.01	-0.39	-2.16	18.82	18.17	-85.04	19.83	17.44	-56.43
135	15969	-0.22	4.01	-0.55	-2.81	20.85	22.53	-89.66	22.34	21.59	-60.53
150	15963	-0.31	4.01	-0.69	-3.57	22.61	25.83	-94.58	24.76	25.05	-64.03
165	15955	-0.41	4.02	-0.80	-4.41	24.80	28.56	-98.91	27.10	27.89	-67.26
180	15960	-0.50	4.02	-0.90	-5.31	26.11	30.75	-103.50	28.96	30.15	-70.63

**Table 8.** Normalized BIAS and forecast skill related to MAE-FSMAE and RMSE-FSRMSE for plant P4 from 15 min up to three hours ahead.

LAG	NUM	nBIAS_AR	nBIAS_ST	nBIAS_SP	nBIAS_PP	FSMAE_AR	FSMAE_ST	FSMAE_PP	FSRMSE_AR	FSRMSE_ST	FSRMSE_PP
15	11339	0.20	-0.65	0.60	-0.01	4.21	-105.53	-22.64	5.80	-71.91	-6.82
30	11334	0.08	-0.65	1.11	-0.07	11.32	-32.43	-31.02	5.79	-20.84	-12.90
45	11328	0.21	-0.65	1.60	-0.15	19.61	-2.57	-36.40	13.83	2.16	-16.31
60	11322	0.25	-0.64	2.03	-0.28	24.69	13.83	-41.88	18.14	14.67	-21.52
75	11324	0.35	-0.62	2.44	-0.47	28.55	25.25	-45.93	22.98	24.39	-25.16
90	11318	0.44	-0.62	2.84	-0.72	32.54	33.68	-49.28	27.40	31.49	-28.68
105	11313	0.42	-0.60	3.25	-1.05	35.63	40.16	-52.03	31.05	37.39	-31.21
120	11311	0.26	-0.59	3.65	-1.46	37.49	45.13	-54.50	33.40	41.95	-33.63
135	11303	0.15	-0.59	3.99	-1.98	39.08	48.98	-56.92	36.02	45.75	-35.49
150	11305	0.06	-0.59	4.35	-2.57	41.24	52.14	-59.02	38.64	48.79	-37.33
165	11307	0.08	-0.59	4.69	-3.25	43.80	54.75	-60.63	41.28	51.52	-38.39
180	11306	-0.10	-0.58	5.05	-3.99	44.73	56.95	-62.21	42.66	53.89	-39.36

In order to give evidence of the usefulness of introducing the *ST* as input of the *VST* the authors have implemented an ARIMAX without using the *ST* prediction as explanatory variable. This new ARIMAX is called *AR1* on the follow.

In general, the performances of *AR1* are substantially lower than *AR* at each time horizon and it also gains worse results than *SP* after few lead times, as can be seen analyzing the progress of *nMAE* and *nRMSE* in Figure 9, related to plant P4. In the figure, the errors related to *AR1* are shown with red lines.

In addition to consider the performance of ARIMAX without the use of *ST* output as exogenous variable, a comparison on the absolute *MAE* of *ST* and *AR* has been considered, in order to analyze the influence of the errors of the *ST* on the final *VST*. For this comparison it is meant that the *VST* is the one obtained from *AR*.

In the upper part of Figure 10, the total absolute errors  $Q^{ST}(\varepsilon_{ST})$ ,  $Q^{VST}(\varepsilon_{ST})$  introduced in Section 2.4 are shown, while the cumulative ones  $C^{ST}(\varepsilon_{ST})$ ,  $C^{VST}(\varepsilon_{ST})$  are reported in the lower part of the same figure, as a function of the *ST* error  $\varepsilon_r^{ST}$ . The graphs on the left of Figure 10a refer to plant P1 and a forecast horizon of  $K = 60$  min, while those on the right of Figure 10b refer to plant P4 and a forecast horizon of  $K = 90$  min. The red lines refer to *VST*, the black ones to *ST* forecasts.

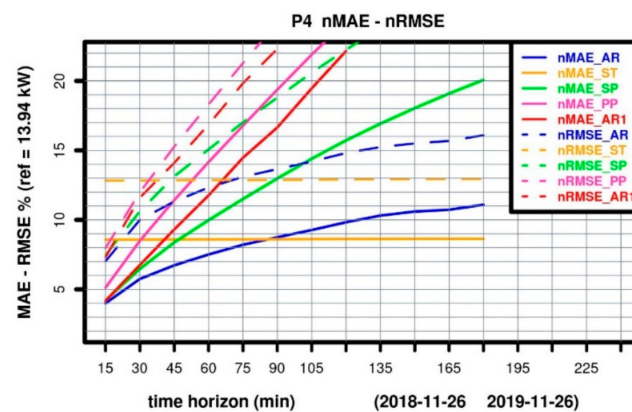


**Figure 9.**  $nMAE$  (solid) and  $nRMSE$  (dashed) errors as a function of the prediction horizon for ARIMAX (AR) in blue, optimized short-term forecasting (ST) in orange, smart persistence (SP) in green, pure persistence (PP) in pink and ARIMAX without ST as input (AR1) in red, related to the plants P4.

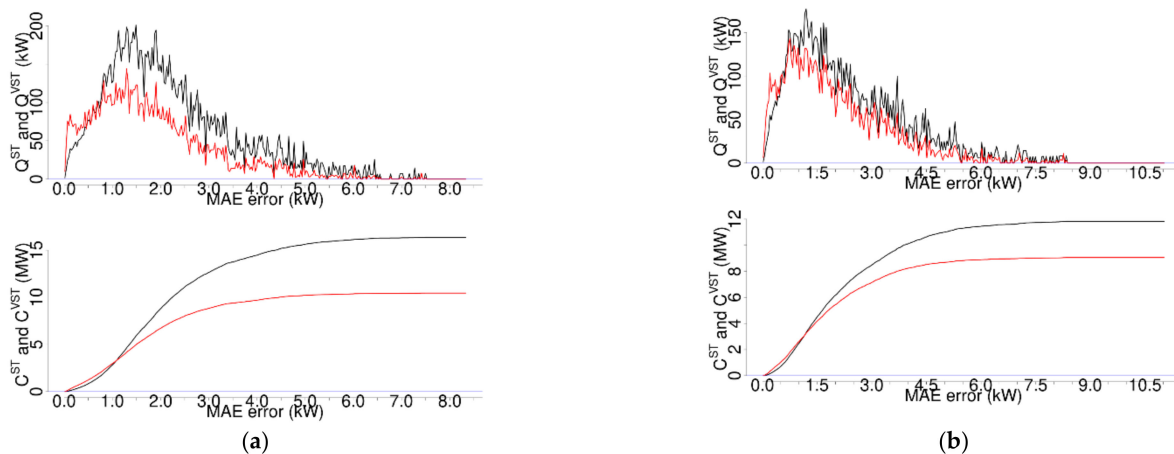


**Figure 10.** Total run time errors  $Q^{ST}(\epsilon_r^{ST})$  in black and  $Q^{VST}(\epsilon_r^{ST})$  in red in the top, cumulative total run-time errors  $C^{ST}(\epsilon_r^{ST})$  and  $C^{VST}(\epsilon_r^{ST})$  in the bottom as a function of the ST error  $\epsilon_r^{ST}$ . (a) P1 with forecast horizon  $K = 60$  min, (b) P4 with forecast horizon  $K = 90$  min (see Equation (17) and Equation (18) in Section 2.4 for details of the errors).

It can be noted that when the ST forecast is accurate, the VST fails to improve the forecast, but the associated amount of error, which is roughly twice that of the ST, is small. It should be noted that low errors can result from accurate forecasts, most often during sunny days, but also when the energy involved is small, more likely for very low sun elevation angles.

When the ST errors increase, the VST errors are definitively smaller than those of the ST, and the cumulative trends show an improvement of about 30% for the 60-min forecast horizons and around 20% for the 90-min horizons. The ability of VST to reduce ST errors is evident for any amount of ST error.

#### 4. Discussion and Conclusions

In this work both a new short-term and a new very-short-term PV power forecasting systems have been implemented and their performances analyzed by means of the application to four small scale grid-connected plants in Italy in the period November 2018–November 2019. The ST model is mainly characterized by a multimodel approach, obtained through the exploitation of the weather forecast derived from different NWP models and an optimal combination of single forecasting systems based on the *AnEn* statistical technique.

The new *VST* system, operated by means of the ARIMAX method, stands out, in particular, for the use of the *ST* prediction, *SP* and *GHI-Sat* as exogenous input.

In the same study a simple, powerful prediction method has been also introduced, that is an “astronomical” correction of the pure persistence, obtained through a normalization of the solar zenith angle along the time.

Both the optimized multimodel *ST* and the *VST* have gained promising results, outperforming the respective references at each time horizon of the forecast. In particular, in terms of nMAE, the *ST* has obtained an improvement at least greater than 30% with respect to the smart persistence, used as baseline and of around 40% in terms of nRMSE, for each of the three day-ahead forecasting horizon.

As regard the *VST* the improvement with respect to the baseline is always relevant, for each horizon and rapidly increases with the time-frame. This successful result derives from the exploitation of the output of the *ST* as exogenous input of ARIMAX, as shown by means of a comparison with another version of ARIMAX, without the use of the *ST* as explanatory variable.

Through the use in combination of the *ST* and *VST* forecasts, a multi-time frames forecasting tool has been realized, covering the horizon from fifteen minutes up to three days ahead with a time resolution of fifteen minutes. Both the *ST* and *VST* are well suited for operational use for their reduced request of computing power. The *VST* is able to start at any time of the day and because of its speed of execution it can supply continuously updated and more accurate forecasts. Both the methods do not require historical and current weather measurements in situ, resulting easy to apply when this information is not available.

The multi-time frame tool has obtained good performances for all the plants, different from each other for size, orientation and climatic conditions of the places where they are installed, proving that they can be generalized and adopted on various plants, with no requirement of specific information on the installation. It is also important to take in account that the methods have been applied to small-scale plants, highly sensitive to changes in cloudiness conditions, therefore further improvements in the performances are expected when applied to larger plants. It is in fact well known the effect of smoothing error due to an increase in spatial scale studied by Pierro et al. [41].

The influence of the weather variability on the performances has been investigated by means of a specific analysis of the cloudiness variation in correspondence of each site. The analysis has confirmed that it is not proper to expect that a PV power forecasting method could obtain the same performances regardless of the meteorology of the place where it is applied. Therefore, it can be useful, in general, to complement the error analysis with a study of the weather conditions of each site.

With regard to the *ST*, other optimization systems are under study, that could lead to further improvements, while for the *VST* other information on the cloudiness, derived from meteorological satellites, not only in correspondence of the site but also in the surroundings, could help to capture irradiance variations in advance.

**Author Contributions:** Conceptualization, E.C. and D.R.; methodology, E.C. and D.R.; software, E.C. and D.R.; validation, E.C. and D.R.; formal analysis, E.C. and D.R.; investigation, E.C. and D.R.; resources, E.C. and D.R.; data curation, E.C. and D.R.; writing—original draft preparation, E.C. and D.R.; writing—review and editing, E.C. and D.R.; visualization, E.C. and D.R.; supervision, E.C. and D.R. All authors have read and agreed to the published version of the manuscript.

**Funding:** This work has been financed by Research Fund for the Italian Electrical System with the Decree of 16 April 2018.

**Acknowledgments:** The authors would like to thank the colleagues Maugeri Giosuè and Guastella Salvatore for supplying the power data to test the described methods, and the reviewers for their valuable comments on the manuscript.

**Conflicts of Interest:** The authors declare no conflict of interest. The funders had no role in the design of the study; in the collection, analyses, or interpretation of data; in the writing of the manuscript, or in the decision to publish the results.

### Abbreviations

In the text lots of abbreviations are used. In order to facilitate the reader, the most used are reported in this section in alphabetical order:

<i>AnEn</i> :	Analog Ensemble
<i>AR</i> :	ARIMAX with ST, SP and GHI-Sat exogenous variables
<i>AR1</i> :	as AR, but without ST as exogenous variables
<i>AZI</i> :	solar azimuth angle
<i>DHI</i> :	diffuse horizontal irradiation
<i>DNI</i> :	direct normal irradiation
<i>ELEV</i> :	solar elevation
<i>GHI</i> :	global horizontal irradiation
<i>GHI-NWP</i> :	<i>GHI</i> derived from <i>NWP</i> model
<i>GHI-Sat</i> :	<i>GHI</i> derived from satellite data
<i>GFS</i> :	Global Forecast System—global <i>NWP</i>
<i>IFS</i> :	Integrated Forecast System—global <i>NWP</i>
<i>NWP</i> :	Numerical Weather Prediction
<i>PP</i> :	Pure power Persistence
<i>PWC</i> :	Precipitable Water Content
<i>RAMS</i> :	Regional Atmospheric Modeling System (regional <i>NWP</i> )
<i>RES</i> :	<i>RAMS</i> initialized with <i>IFS</i>
<i>RGN</i> :	<i>RAMS</i> initialized with <i>GFS</i>
<i>RHU</i> :	Relative Humidity
<i>SP</i> :	Smart power Persistence
<i>ST</i> :	Short Term power forecast
<i>TEMP</i> :	air TEMPerature
<i>TPAN</i> :	PANel Temperature
<i>VST</i> :	Very Short-Term power forecast
<i>WES</i> :	<i>WRF</i> initialized with <i>IFS</i>
<i>WGN</i> :	<i>WRF</i> initialized with <i>GFS</i>
<i>WRF</i> :	Weather Research and Forecasting Model (regional <i>NWP</i> )
<i>WS</i> :	Wind Speed at 10 m above the ground

### Appendix A

In this section some considerations about the distribution of the cloudiness on the four analyzed plants are summarized. The analysis has been performed exploiting the cloud classification obtained from satellite data, every fifteen minutes, on the satellite pixels nearest to each plant, during the period November 2018–November 2019. Only day-time data have been considered in the analysis.

The purpose of this deepening is a critical evaluation of the *VST* forecasting performances and of the appropriateness in considering both the smart power persistence and the *GHI-Sat* exogenous variables for the *VST* horizon, in the light of the general conditions of the sky over the plants.

There are two features to consider: the temporal persistence and the spatial homogeneity of the cloudiness. The former is an indicator of the reliability of the smart power persistence, while the latter can facilitate the understanding of the reasons behind the peculiar behaviors of the *VST* for some plants.

For the sake of simplicity, the CT types described in Table 2 have been grouped in two class:

- clear, that is the case CT = 1 (cloud-free land);
- cloudy, resulting from merging the CT types between 5 and 19 (different typologies of clouds, see Table 2).

When the temporal horizon equals to 0, a description of the initial condition is given. Considering the dimension of the data set of at least 12,000 time points, the temporal horizon 0 can be considered representative of the general cloudiness conditions of each site.

Considering the general sky conditions, in Figure A1 there are shown the fractional amounts of clear and cloudy sky conditions for the four PV plants at the starting time of the four VST forecasts. The bar plots on the left of Figure A1a have been obtained considering the central point of a grid  $3 \times 3$  of MSG pixels just over the plant location, while on the right (b) there are displayed the percentages achieved using the modal value of the cloudiness in the same grid. It is interesting to note the strong different percentages for the P4 plant, where it happens that there were more clear sky points around that above the zenith of the point.

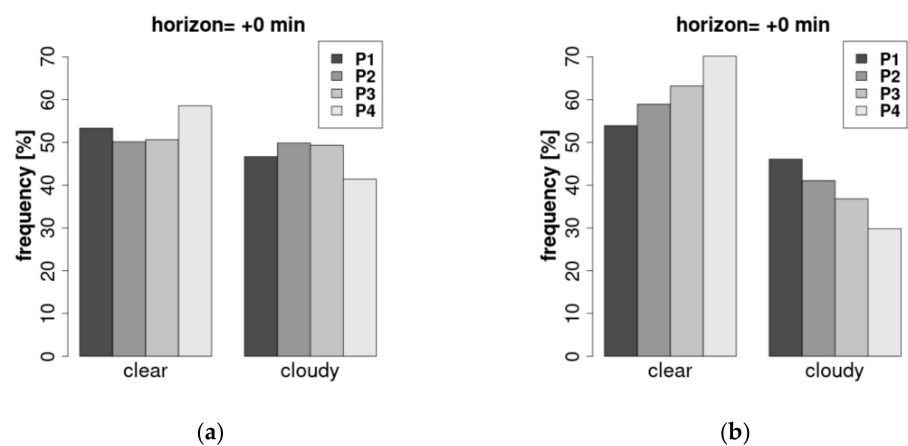


**Figure A1.** Bar plots regarding the amount of clear and cloudy sky conditions at the starting time for the four PV plants. In (a) the fraction of clear and cloudy conditions using the central MSG point, in (b) the corresponding values obtained using the mode value over a box  $3 \times 3$  points.

This inhomogeneity could give rise to criticalities in the VST forecasting. In fact, considering flat planes, power production is mainly affected by global irradiation, sum of the diffuse and direct irradiation components, dependent from the cloudiness over the plant, but also with a contribution from surrounding pixels. In case of large differences between the cloudiness on the central pixel and the nearby, a worsening in the GHI-Sat estimation is expected, because the cloud classification of the pixel over the plant could be drastically different from the ones of the surrounding pixels and also less related with the production. Because of the GHI-Sat is one of the predictors of ARIMAX, in this situation a worsening in the VST is expected. On the contrary, in presence of spatial homogeneity, better performance of VST is expected, as in the case of the plant P1 that shows the largest spatial homogeneity in terms of cloudiness.

The temporal persistence can be examined considering the amount of clear and of cloudy situations that remain unchanged after 3 h. In Figure A2 on the left (a) the unchanged clear and cloudy conditions are shown for the four PV plants, while (b) shows the temporal decreasing of the clear percentages that remained unchanged after 180 min (labelled with p) in the plot, and the percentages that changed their CT typology in 3 h (labelled with n) in the plot.

In Table A1 the total unchanged (clear that remains clear plus cloudy that remains cloudy) percentages are summarised.

While P1 and P3 have almost the same value if the central point or the mode are used, implying that the contribution to surface radiation becoming from the central or around it is quite the same, P2 and P4 show about 5 percentage points difference between the central and the modal values. The larger worsening in SP for P4 is due to its higher percentage of clear sky conditions at time = +0 in combination with the marked difference between central point and mode.

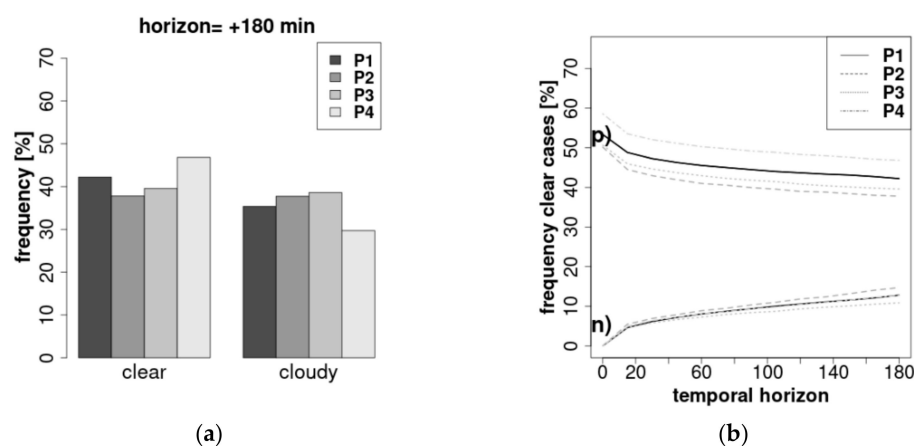


**Figure A2.** (a) bar plots regarding the amount of clear and cloudy which maintained their condition after 180 min; (b) temporal variation of the clear persistent cases (lines labelled with p) and of those that changed their status after 180 min (labelled with n).

**Table A1.** Percentage of cases that does not change their CT typology after 180 min for the four PV plants, using the central MSG point or the modal value in the box of  $3 \times 3$  pixels.

Horizon = +180 m	P1	P2	P3	P4
Central MSG point	77.60%	75.55%	78.20%	76.53%
Mode value	78.29%	80.21%	79.92%	81.30%

## References

- Renewables 2020 Global Status Report; REN21: Paris, France, 2020; ISBN 978-3-948393-00-7.
- IEA. *Global Energy Review 2020 The Impact of COVID-19 Crisis on Global Demand and CO<sub>2</sub> Emissions*; IEA: Paris, France, 2020.
- Antonanzas, J.; Osorio, N.; Escobar, R.; Urraca, R.; Martinez-de-Pison, F.J.; Antonanzas-Torres, F. Review of Photovoltaic Power Forecasting. *Sol. Energy* **2016**, *136*, 78–111. [\[CrossRef\]](#)
- Reindl, T.; Walsh, W.; Yanqin, Z.; Bieri, M. Energy Meteorology for Accurate Forecasting of PV Power Output on Different Time Horizons. *Energy Procedia* **2017**, *130*, 130–138. [\[CrossRef\]](#)
- Das, U.K.; Tey, K.S.; Seyedmahmoudian, M.; Mekhilef, S.; Idris, M.Y.I.; Van Deventer, W.; Horan, B.; Stojcevski, A. Forecasting of Photovoltaic Power Generation and Model Optimization: A Review. *Renew. Sustain. Energy Rev.* **2018**, *81*, 912–928. [\[CrossRef\]](#)
- Wan, C.; Zhao, J.; Song, Y.; Xu, Z.; Lin, J.; Hu, Z. Photovoltaic and Solar Power Forecasting for Smart Grid Energy Management. *CSEE J. Power Energy Syst.* **2015**, *1*, 38–46. [\[CrossRef\]](#)
- Bessa, R.J.; Möhrlen, C.; Fundel, V.J.; Siefert, M.; Browell, J.; Gaidi, S.H.E.; Hodge, B.-M.; Cali, U.; Kariniotakis, G. Towards Improved Understanding of the Applicability of Uncertainty Forecasts in the Electric Power Industry. Available online: [/paper/Towards-Improved-Understanding-of-the-Applicability-Bessa-M%C3%B6hrlen/ed58b2e311ad1e9c05055d13107840ea2b1ab18d](#) (accessed on 17 July 2020).
- Mellit, A.; Pavan, M.; Oglari, E.; Leva, S.; Lughi, V. Advanced Methods for Photovoltaic Output Power Forecasting: A Review. *Appl. Sci.* **2020**, *10*, 487. [\[CrossRef\]](#)
- Ahmed, R.; Sreeram, V.; Mishra, Y.; Arif, M.D. A Review and Evaluation of the State-of-the-Art in PV Solar Power Forecasting: Techniques and Optimization. *Renew. Sustain. Energy Rev.* **2020**, *124*, 109792. [\[CrossRef\]](#)
- Dolara, A.; Leva, S.; Manzolini, G. Comparison of Different Physical Models for PV Power Output Prediction. *Sol. Energy* **2015**, *119*, 83–99. [\[CrossRef\]](#)
- Dutta, S.; Li, Y.; Venkataraman, A.; Costa, L.M.; Jiang, T.; Plana, R.; Tordjman, P.; Choo, F.H.; Foo, C.F.; Puttgen, H.B. Load and Renewable Energy Forecasting for a Microgrid Using Persistence Technique. *Energy Procedia* **2017**, *143*, 617–622. [\[CrossRef\]](#)
- Barbieri, F.; Rajakaruna, S.; Ghosh, A. Very Short-Term Photovoltaic Power Forecasting with Cloud Modeling: A Review. *Renew. Sustain. Energy Rev.* **2017**, *75*, 242–263. [\[CrossRef\]](#)
- Zhou, H.; Zhang, Y.; Yang, L.; Liu, Q.; Yan, K.; Du, Y. Short-Term Photovoltaic Power Forecasting Based on Long Short Term Memory Neural Network and Attention Mechanism. *IEEE Access* **2019**. [\[CrossRef\]](#)
- Pedro, H.T.C.; Coimbra, C.F.M. Assessment of Forecasting Techniques for Solar Power Production with No Exogenous Inputs. *Sol. Energy* **2012**, *86*, 2017–2028. [\[CrossRef\]](#)
- Ahmad, W.; Ahmad, S. Arima Model and Exponential Smoothing Method: A Comparison. *AIP Conf. Proc.* **2013**, *1522*, 1312–1321. [\[CrossRef\]](#)

16. Nobre, A.M.; Severiano, C.A.; Karthik, S.; Kubis, M.; Zhao, L.; Martins, F.R.; Pereira, E.B.; R  ther, R.; Reindl, T. PV Power Conversion and Short-Term Forecasting in a Tropical, Densely-Built Environment in Singapore. *Renew. Energy* **2016**, *94*, 496–509. [[CrossRef](#)]
17. Bacher, P.; Madsen, H.; Nielsen, H.A. Online Short-Term Solar Power Forecasting. *Sol. Energy* **2009**, *83*, 1772–1783. [[CrossRef](#)]
18. Perez-Mora, N.; Mart  nez Moll, V.; Canals, V. Spanish Renewable Energy Generation Short-Term Forecast. In Proceedings of the ISES Solar World Congress 2015, Daegu, Korea, 8–12 November; Volume 1, p. 216.
19. Li, Y.; Su, Y.; Shu, L. An ARMAX Model for Forecasting the Power Output of a Grid Connected Photovoltaic System. *Renew. Energy* **2014**, *66*, 78–89. [[CrossRef](#)]
20. Samuel, A.L. Some Studies in Machine Learning Using the Game of Checkers. *IBM J. Res. Dev.* **1959**, *3*, 210–229. [[CrossRef](#)]
21. Leva, S.; Dolara, A.; Grimaccia, F.; Mussetta, M.; Ogliari, E. Analysis and Validation of 24 Hours Ahead Neural Network Forecasting of Photovoltaic Output Power. *Math. Comput. Simul.* **2017**, *131*, 88–100. [[CrossRef](#)]
22. Gutierrez-Corea, F.-V.; Manso-Callejo, M.-A.; Moreno-Regidor, M.-P.; Manrique-Sancho, M.-T. Forecasting Short-Term Solar Irradiance Based on Artificial Neural Networks and Data from Neighboring Meteorological Stations. *Sol. Energy* **2016**, *134*, 119–131. [[CrossRef](#)]
23. Deng, L.; Yu, D. *Deep Learning for Signal and Information Processing*; Microsoft Res. Monogr, Microsoft Research: Redmond, WA, USA, 2013.
24. Wang, K.; Qi, X.; Liu, H. A Comparison of Day-Ahead Photovoltaic Power Forecasting Models Based on Deep Learning Neural Network. *Appl. Energy* **2019**, *251*, 113315. [[CrossRef](#)]
25. Gao, M.; Li, J.; Hong, F.; Long, D. Day-Ahead Power Forecasting in a Large-Scale Photovoltaic Plant Based on Weather Classification Using LSTM. *Energy* **2019**, *187*, 115838. [[CrossRef](#)]
26. Zhang, J.; Verschae, R.; Nobuhara, S.; Lalonde, J.-F. Deep Photovoltaic Nowcasting. *Sol. Energy* **2018**, *176*, 267–276. [[CrossRef](#)]
27. Ehsan, R.M.; Simon, S.P.; Venkateswaran, P.R. Day-Ahead Forecasting of Solar Photovoltaic Output Power Using Multilayer Perceptron. *Neural Comput. Appl.* **2017**, *28*, 3981–3992. [[CrossRef](#)]
28. Abdel-Nasser, M.; Mahmoud, K. Accurate Photovoltaic Power Forecasting Models Using Deep LSTM-RNN. *Neural Comput. Appl.* **2019**, *31*, 2727–2740. [[CrossRef](#)]
29. Li, G.; Wang, H.; Zhang, S.; Xin, J.; Liu, H. Recurrent Neural Networks Based Photovoltaic Power Forecasting Approach. *Energies* **2019**, *12*, 2538. [[CrossRef](#)]
30. Van der Meer, D.W.; Wid  n, J.; Munkhammar, J. Review on Probabilistic Forecasting of Photovoltaic Power Production and Electricity Consumption. *Renew. Sustain. Energy Rev.* **2018**, *81*, 1484–1512. [[CrossRef](#)]
31. Lauret, P.; David, M.; Pedro, H.T. Probabilistic Solar Forecasting Using Quantile Regression Models. *Energies* **2017**, *10*, 1591. [[CrossRef](#)]
32. Kim, C.K.; Kim, H.-G.; Kang, Y.-H.; Yun, C.-Y.; Kim, S.Y. Probabilistic Prediction of Direct Normal Irradiance Derived from Global Horizontal Irradiance over the Korean Peninsula by Using Monte-Carlo Simulation. *Sol. Energy* **2019**, *180*, 63–74. [[CrossRef](#)]
33. Sun, M.; Feng, C.; Zhang, J. Probabilistic Solar Power Forecasting Based on Weather Scenario Generation. *Appl. Energy* **2020**, *266*, 114823. [[CrossRef](#)]
34. Alessandrini, S.; Delle Monache, L.; Sperati, S.; Cervone, G. An Analog Ensemble for Short-Term Probabilistic Solar Power Forecast. *Appl. Energy* **2015**, *157*, 95–110. [[CrossRef](#)]
35. Poulek, V.; Dang, M.Q.; Libra, M.; Ber  nek, V.; Safr  nkov  , J. PV Panel with Integrated Lithium Accumulators for BAPV Applications—One Year Thermal Evaluation. *IEEE J. Photovolt.* **2020**, *10*, 150–152. [[CrossRef](#)]
36. Diagne, M.; David, M.; Lauret, P.; Boland, J.; Schmutz, N. Review of Solar Irradiance Forecasting Methods and a Proposition for Small-Scale Insular Grids. *Renew. Sustain. Energy Rev.* **2013**, *27*, 65–76. [[CrossRef](#)]
37. Cai, C.; Aliprantis, D.C. Cumulus Cloud Shadow Model for Analysis of Power Systems with Photovoltaics. *IEEE Trans. Power Syst.* **2013**, *28*, 4496–4506. [[CrossRef](#)]
38. Liu, L.; Zhao, Y.; Chang, D.; Xie, J.; Ma, Z.; Sun, Q.; Yin, H.; Wennersten, R. Prediction of Short-Term PV Power Output and Uncertainty Analysis. *Appl. Energy* **2018**, *228*, 700–711. [[CrossRef](#)]
39. Mishra, S.; Palanisamy, P. Multi-Time-Horizon Solar Forecasting Using Recurrent Neural Network. In Proceedings of the 2018 IEEE Energy Conversion Congress and Exposition (ECCE), Portland, OR, USA, 23–27 September 2018; pp. 18–24.
40. Carriere, T.; Vernay, C.; Pitaval, S.; Kariniotakis, G. A Novel Approach for Seamless Probabilistic Photovoltaic Power Forecasting Covering Multiple Time Frames. *IEEE Trans. Smart Grid* **2020**, *11*, 2281–2292. [[CrossRef](#)]
41. Pierro, M.; Cornaro, C.; Moser, D.; Betti, A.; Moschella, M.; Collino, E.; Ronzio, D. Regional Solar Power Forecasting, IEA-PVPS. 2020. Available online: [https://iea-pvps.org/wp-content/uploads/2020/07/IEA\\_PVPS\\_T16\\_regional\\_forecast.pdf](https://iea-pvps.org/wp-content/uploads/2020/07/IEA_PVPS_T16_regional_forecast.pdf) (accessed on 1 February 2021).
42. Skamarock, C.; Klemp, B.; Dudhia, J.; Gill, O.; Barker, D.; Duda, G.; Huang, X.; Wang, W.; Powers, G. A Description of the Advanced Research WRF Version 3. 2008. Available online: <https://opensky.ucar.edu/islandora/object/technotes%3A500/datastream/PDF/view> (accessed on 1 February 2021).
43. Pielke, R.A.; Cotton, W.R.; Walko, R.L.; Tremback, C.J.; Lyons, W.A.; Grasso, L.D.; Nicholls, M.E.; Moran, M.D.; Wesley, D.A.; Lee, T.J.; et al. A Comprehensive Meteorological Modeling System—RAMS. *Meteorol. Atmospheric Phys.* **1992**, *49*, 69–91. [[CrossRef](#)]

44. Kühnert, J.; Lorenz, E.; Heinemann, D.; Kleissl, J. Chapter 11-satellite-based irradiance and power forecasting for the German energy market. In *Solar Energy Forecasting and Resource Assessment*; Academic Press: Boston, MA, USA, 2013; Volume 11, pp. 267–297, ISBN 978-0-12-397177-7.
45. Yu, D.; Lee, S.; Lee, S.; Choi, W.; Liu, L. Forecasting Photovoltaic Power Generation Using Satellite Images. *Energies* **2020**, *13*, 6603. [[CrossRef](#)]
46. Schmetz, J.; Pili, P.; Tjemkes, S.; Just, D.; Kerkmann, J.; Rota, S.; Ratier, A. An Introduction To Meteosat Second Generation (MSG). *Bull. Am. Meteorol. Soc.* **2002**, *83*, 977–992. [[CrossRef](#)]
47. Herve Le Gleau Algorithm Theoretical Basis Document for the Cloud Product Processors of the NWC/GEO. 2016. Available online: [https://www.nwcsaf.org/documents/20182/30662/NWC-CDOP2-GEO-MFL-SCI-ATBD-Cloud\\_v1.1.pdf/a5bb6eca-871b-4707-9c76-e0be09915d94](https://www.nwcsaf.org/documents/20182/30662/NWC-CDOP2-GEO-MFL-SCI-ATBD-Cloud_v1.1.pdf/a5bb6eca-871b-4707-9c76-e0be09915d94) (accessed on 1 February 2021).
48. Elena Collino Exploiting of NWC GEO CT and EXIM Packages for Irradiation Estimation: Analysis and Validation. 2020. Available online: [https://www.nwcsaf.org/Downloads/Workshop2020/Presentations/Session\\_X/4.NWCSAF\\_CT\\_EXIM\\_Collino\\_UsersWS2020.pdf](https://www.nwcsaf.org/Downloads/Workshop2020/Presentations/Session_X/4.NWCSAF_CT_EXIM_Collino_UsersWS2020.pdf) (accessed on 1 February 2021).
49. Dambreville, R.; Blanc, P.; Chanussot, J.; Boldo, D. Very Short-Term Forecasting of the Global Horizontal Irradiance Using a Spatio-Temporal Autoregressive Model. *Renew. Energy* **2014**, *72*, 291–300. [[CrossRef](#)]
50. Delle Monache, L.; Eckel, F.; Rife, D.; Nagarajan, B.; Searight, K. Probabilistic Weather Prediction with an Analog Ensemble. *Mon. Weather Rev.* **2013**, *141*, 3498–3516. [[CrossRef](#)]
51. Kioutsioukis, I.; Galmarini, S. De Praeceptis Ferendis: Good Practice in Multi-Model Ensembles. *Atmospheric Chem. Phys.* **2014**, *14*, 11791–11815. [[CrossRef](#)]
52. Collino, E.; Ronzio, D.; Bonanno, R.; Partasides, G. Evaluation of Different PV Power Forecasting Systems on Grid-Connected PV Plants in the Mediterranean Area. In Proceedings of the 2019 1st International Conference on Energy Transition in the Mediterranean Area (SyNERGY MED), Cagliari, Italy, 28–30 May 2019; 2019; pp. 1–6.
53. Skoplaki, E.; Palyvos, J.A. On the temperature dependence of photovoltaic module electrical performance: A review of efficiency/power correlations. *Sol. Energy* **2009**, *83*, 614–624. [[CrossRef](#)]
54. Box, G.E.P.; Jenkins, G.M. *Time Series Analysis: Forecasting and Control, Revised Ed*; Holden-Day Series in Time Series Analysis and Digital Processing; Holden-Day: San Francisco, CA, USA, 1976; ISBN 0-8162-1104-3.
55. Yang, D.; Kleissl, J.; Gueymard, C.A.; Pedro, H.T.C.; Coimbra, C.F.M. History and Trends in Solar Irradiance and PV Power Forecasting: A Preliminary Assessment and Review Using Text Mining. *Sol. Energy* **2018**, *168*, 60–101. [[CrossRef](#)]
56. Hyndman, R.J.; Khandakar, Y. Automatic Time Series Forecasting: The Forecast Package for R. *J. Stat. Softw.* **2008**, *27*, 1–22. [[CrossRef](#)]
57. Cort, J. Willmott; Kenji Matsuura Advantages of the Mean Absolute Error (MAE) over the Root Mean Square Error (RMSE) in Assessing Average Model Performance. *Clim. Res.* **2005**, *30*, 79–82.
58. Botchkarev, A. A New Typology Design of Performance Metrics to Measure Errors in Machine Learning Regression Algorithms. *Interdiscip. J. Inf. Knowl. Manag.* **2019**, *14*, 45–79. [[CrossRef](#)]
59. Chai, T.; Draxler, R.R. Root Mean Square Error (RMSE) or Mean Absolute Error (MAE)? Arguments against Avoiding RMSE in the Literature. *Geosci. Model Dev.* **2014**, *7*, 1247–1250. [[CrossRef](#)]